First SedAlp Milestone

WP5 - Action 5.2

Protocol for data collection method in sediment transport

June, 2013

Introduction

The main objective of the SedAlp project is to develop tools and strategies for an integrated sediment management. To reach this ambitious goal, it is elementary to understand the behaviour and characteristics of sediment transport. The knowledge about this complex natural process is still limited, therefore field observations and data on sediment transport are needed. Work package 5 (WP5), with the title “Sediment transport monitoring”, basically aims on providing this data to expand the understanding of sediment transport, debris flows and wood transport.

Throughout the whole Alpine Region, a lot of different monitoring methods in sediment transport are currently in use. The presented first SedAlp Milestone, with the title “Protocol for data collection method in sediment transport”, aims on ensuring the comparability of the collected monitoring data.

Therefore, three standard protocols on bedload transport, debris flow and wood transport monitoring have been developed. These protocols are intended to describe the used monitoring technics and data processing methods. Furthermore, the protocols work also as guidelines to assist in choosing the appropriate monitoring method for supporting prospective monitoring efforts.

Contents

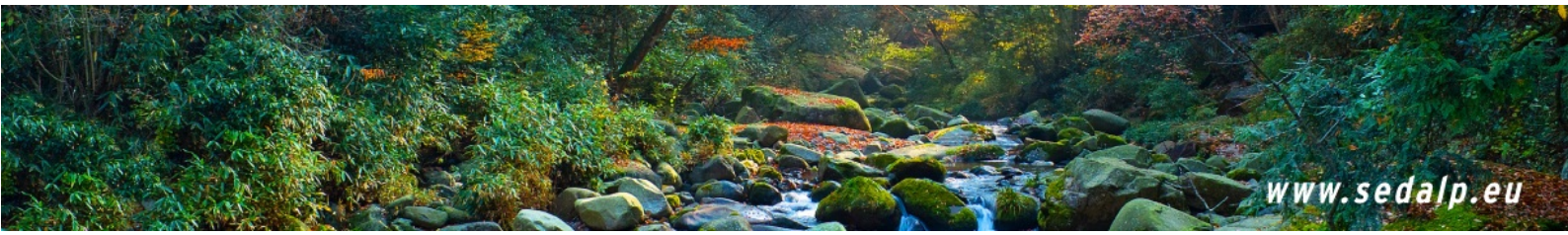

Part I

Protocol for Bedload Monitoring

WP5 - Action 5.2

Protocols on standardized data collection methods in sediment transport monitoring for transboundary exchange

Lead authors: Johann Aigner, Andrea Kreisler & Helmut Habersack (PP11), Francesco Comiti (PP1)

Contributors: Tobias Heckmann, Judith Abel, Florian Haas & Michael Becht (PP6), Frédéric Liébault (PP7), Matteo Cesca & Alessandro Vianello (PP2)

June, 2013

www.sedalp.eu

Sediment management in Alpine basins

Contents

1 Introduction

The movement of sediment particles on or close to the riverbed by rolling, sliding or saltation is called bedload transport. Field-derived knowledge data of bedload transport is required to adequately plan flood protection and torrent control systems, waterway management and in general river engineering works. Furthermore, quantification of bedload transport is needed for issues concerning ecosystem dynamics and hydropower management. From relatively low to flood flows, bedload transport features a dramatic spatio-temporal variability and a fairly stochastic behaviour (Habersack et al., 2008). Therefore, field measurements are essential to select, apply and calibrate bedload transport formulas and numerical models. Nonetheless, measuring bedload transport in natural rivers is still a challenging task.

Several different methods are currently used for bedload monitoring worldwide. They all have advantages and disadvantages, thus in many instances it is recommended to combine different methods to achieve the desired goals. The integrative monitoring system presented in Habersack et al (2013, in prep.) shows an example in the use of complementary bedload monitoring methods.

The following protocol will give an overview about the different bedload monitoring methods, with more details on those deployed within the Project SedAlp. Furthermore, it should assist in choosing the appropriate monitoring method for questions related to the quantification of bedload transport.

Bedload monitoring methods can be divided into two groups:

- Direct methods
  - Suspended basket samplers
  - Bunte traps
  - Slot traps/samplers
  - Monitored retention basins

- indirect methods
  - Passive acoustics (geophone plates, Japanese acoustic pipe, hydrophones)
  - Active acoustic (ADCP)
  - Tracers (painted, magnetic, PITs…)
  - Topographic/geomorphological (repeated laser scanning or photogrammetry, scour chains…)

2 Bedload Monitoring Methods

Table 1 gives an overview over the main parameters of interest in bedload transport and monitoring methods.

Table 1 Main parameters and monitoring methods

Specific bedload rate	$[kg\ m^{-1}s^{-1}]$
Basket sampler (cross-Section wise measurement, repeated measurement), Bedload trap	
Bedload rate	$[kg\ s^{-1}]$
Basket sampler (cross-Section wise measurement)	
Bedload yield	$[kg]$
Basket sampler (cross-section wise measurement)	
Spatial variability of bedload transport	
Basket sampler (cross-Section wise measurement), geophone plates, Acoustic pipe sensor	
Temporal variability of bedload transport	
Basket sampler (interval measurement), geophone plates, Acoustic pipe sensor	
Initiation of motion	$[m;m^3s^{-1};Nm^{-2}]$
Basket sampler (repeated measurement), Bedload trap, geophone plates, Acoustic pipe sensor, Tracers	
Grain size distribution (sieving required)	
Basket sampler, Bedload trap	
Transport path, Transport velocity	$[m;\ m\ s^{-1}]$
Tracers	
variation of sediment storage	$[m;\ m^3]$
Scour chains, Terrestrial Laser scanning, Aerial Imagery	

2.1 Mobile Basket sampler

Bedload measurements with basket samplers are one of the oldest and most common methods of bedload monitoring (Mühlhofer, 1933; Helley and Smith, 1971).

The concept of basket sampler measurements is relatively simple. A net is fixed on a rectangular metal frame and lowered to the river bed. Bedload material which passes through the frame gets captured in the net. The minimum sediment size which can be sampled is defined by the size of the net holes. The maximum sediment size is limited by the intake width of the sampler. After sampling, the sampled bedload material is dried, weighted and sieved. With the known measuring time and the intake width, the specific (i.e., per unit channel width) bedload transport rate can be calculated.

Different river types require different basket samplers due to their characteristic sediment size, transport intensity and hydraulic conditions. Important aspects in the use of basket sampler are the hydraulic efficiency (back pressure) and possible errors arising from an imperfect use of the basket (over- and under-sampling). Over time several different basket samplers have been developed. Scientific publications are treating topics like, the calibration of bedload samplers, sources of error and their effects of the achieved results and analyses of caught bedload material texture (e.g. Emmett, 1980; Gaudet et al., 1994; Vericat et al., 2006; Habersack & Laronne, 2001).

2.1.1 Large Helley-Smith sampler (LHS)

One of the most commonly used basket samplers is the Large Helley Smith (LHS) sampler presented by Helley and Smith (1971). It is a pressure difference sampler with an intake width of 0.152 m x 0.152 m. Different mesh sizes of sampler nets are adopted (0.25 mm, 0.5 mm, 1 mm, 2 mm…) depending on the sampling objective and river type. Sources of error and their effects of the achieved results in the use of LHS basket sampler can be found in Vericat et al. (2006).

The LHS basket sampler is lowered to the riverbed with a crane (mounted on a trailer or truck), a river cableway or held directly by hand if wading is possible (small streams). Figure 1 and Figure 2 show some examples of the handling of the LHS basket sampler in Dellach/Drau in Austria.

Figure 1 Trailer with crane and LHS basket sampler, Dellach/Drau (Aigner, 2013)

Figure 2 LHS basket sampler, Dellach/Drau (Aigner, 2012)

2.1.2 TIWAG sampler

The TIWAG basket sampler (Figure 3) was constructed by the Austrian Hydropower company TIWAG for bedload transport measurements in Mountain Rivers. The intake width is 0.5 m x 0.5 m, the metal grid which captures the bedload has a mesh size of 8 mm. The relatively large mesh size is necessary to assure the hydraulic efficiency.

A metal pillar defines the exact position of the bedload measurement. During measurements, the sampler is inserted into the metal pillar by a mobile crane and lowered to the riverbed (Figure 4). With this method only interval measurements of bedload transport can be undertaken. When the sampler is positioned behind a geophone plate, the latter can be accurately calibrated.

Figure 3 TIWAG basket sampler behind plate geophones, Lienz/Isel, Austria (Seitz, 2009)

Figure 4 TIWAG sampler lowered by crane Lienz/Isel, Austria (Seitz, 2009)

2.1.3 Vent sampler

The Vent basket sampler (Figure 6) was constructed by BOKU (Vienna) and can be seen as a crane-suspended Bunte trap (see 2.1.6) having different dimensions. It was built for bedload measurements in mountain streams with intense bedload transport (Habersack et al., 2012). The sampler consists of three parts: a rectangular steel-frame (0.44 m x 0.26 m), a sampler bag with a mesh size of 3.5 mm x 6.5 mm and a vertical steel bar. The steel bar is attached, so that the frame can turn into the flow self-adjusting based on the prevailing direction. The sampler can be mounted on a mobile crane at the shackle at the upper end of the steel bar. To prevent the sampler from moving downstream, two tether lines are fixed at the loops on the sides of the frame and on both riverbanks.

Figure 5 Bedload measurement with the Vent basket sampler and a mobile crane, Vent/Rofenache (Aigner, 2012)

Figure 6 Vent basket sampler (Seitz, 2010)

2.1.4 BUNTE traps

"Bunte" traps are portable sampler developed to facilitate sampling irregular and infrequent gravel and small cobble over a wide range of transport rates in wadeable mountain streams (Bunte et al., 2004). The development was a joint effort between the Colorado State University (CSU), Engineering Research Center and the USDA Forest Service (FS), Stream System Technology Center.

Original "Bunte" traps have a 0.3m x 0.2m aluminum frame as the sampler opening, allowing coarse gravel and small cobble particles to enter the trap. The frame has a trailing net with a 4 mm mesh that stores the collected gravel bedload. The net, typically about 1 m long, can be opened, emptied, and closed from the back. These traps are placed on ground plates anchored to the stream bottom with metal stakes. Adjustable nylon webbing straps are used to fasten the frame to the stakes. Ground plates prevent involuntary particle entrainment at the sampler entrance and ensure that all particles that have moved onto the ground plate will enter the trap (Bunte et al., 2007). Indeed, the correct positioning of ground plates is crucial in ensuring a good performance of these traps, making Bunte traps generally more reliable and accurate than Helley-Smith samplers (used without plates) in gravel bed rivers (Bunte et al., 2008).

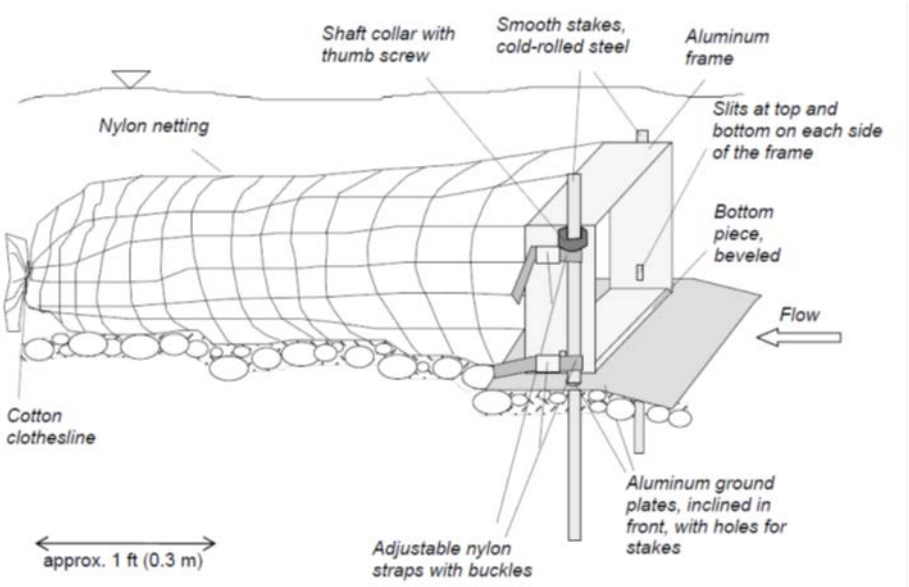

Figure 7 Sketch of a Bunte trap (from Bunte et al. 2007)

The combination of large opening, large sampler capacity, installation on ground plates, and long sampling times are essential for obtaining representative samples of gravel and cobble bedload transport. Because these attributes are more typical of a trap than a sampler, the developers

used the term “bedload trap”, even though the device is not installed below the bed surface as the slot traps described in the following section. For detailed information on the construction and use of the “Bunte” traps, please refer to Bunte et al. (2007).

Figure 8 Left: Bunte traps can be left unmanned in relatively slow flows (from Bunte et al., 2007). Right: in fast turbulent streams the traps are ensured to be in perfect contact with the ground plate by keeping a foot on the upper side of the frame during the sampling time (Saldur River, Italy).

Recently, Kociuba et al. (2012) developed a variation of the “Bunte” traps where multiple samplers can be operated by a single operator standing on a river bank. For more information on this “River bedload trap”, see http://www.freepatentsonline.com/EP2333161.html. Bunte traps have proven quite effective in determining bedload transport rates and sediment mobility up to bankfull conditions in wadable gravel- and cobble-bed streams (Bunte et al., 2004; Bunte et al., 2010; Dell’Agnese et al., 2012) as well as to calibrate an acoustic pipe sensor installed in a mountain river (Dell’Agnese et al., 2013).

2.1.5 Sampling procedures

Cross-section measurements

More bedload measurements across a river section are necessary both to gain information about the spatial variability of specific bedload transport rate (kg m s^{-1}) and to calculate the total bedload transport rate (kg s^{-1}) through a section.

A river cross-section is divided into different verticals based on hydraulic and morphological considerations, which represent the locations where basket sampler is deployed on the bed.

The number of measured verticals varies with river width. On one side, the more verticals are measured, the more accurate will be the calculated bedload transport and the better is the knowledge about the spatial variability of bedload transport. On the other hand, hydraulic conditions should not change during the measurement, which limits the number of verticals. Figure 9 shows an example of a cross section measurement at the Drau river in Dellach (Austria) undertaken with a Large Helley Smith basket sampler. To account for temporal variations in bedload transport three measurements per vertical are recommended (Habersack et al., 2008).

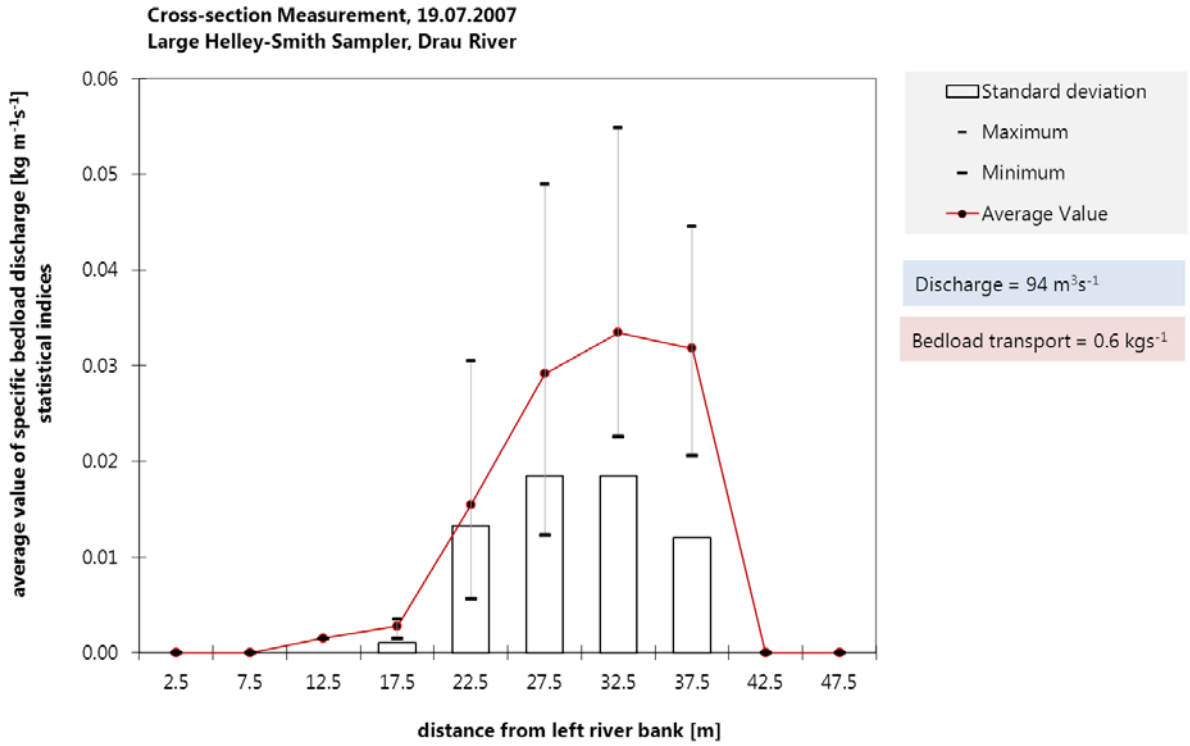

Figure 9 Cross section measurement with the Large Helley-Smith Sampler at Dellach / Drau (Habersack et al., 2008).

Repeated measurements

As mentioned above, bedload transport often shows a strong temporal variability even for constant hydraulic conditions. Repeated measurements at the same vertical are undertaken to capture and quantify such variability. Therefore single basket sampler measurements are repeated at the same vertical over a long period of time. A possible outcome of interval measurements is presented in Figure 10 and shows the temporal variability at a given vertical at Dellach/Drau (Habersack et al., 2008).

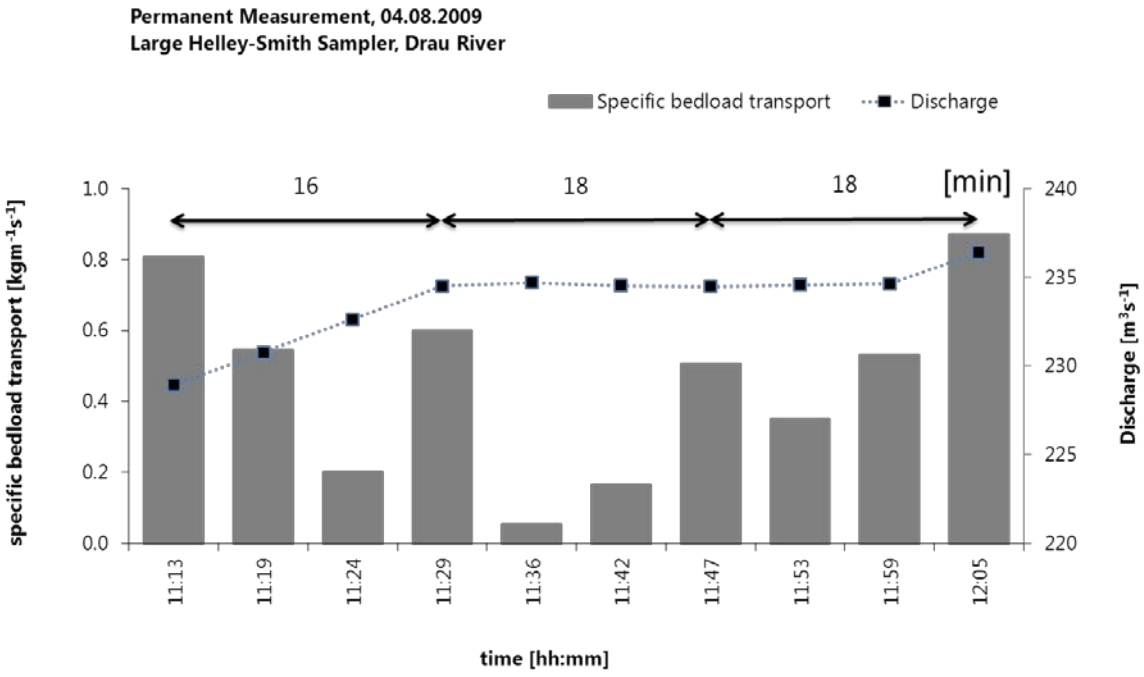

Figure 10 repeated measurement with the Large Helley-Smith Sampler at Dellach/Drau (Habersack et al., 2008).

2.2 Slot traps

This direct bedload monitoring system permits continuous bedload measurements at predefined locations within a cross-section (Reid et al., 1980; Habersack et al., 2010). The slot trap consists of a sample container, covered by a slotted plate and inserted in a formed (concrete) pit in the riverbed. To start bedload sampling the slot is opened (hydraulically via manual control or by hand), enabling bedload material to be trapped into the container. Load cells or a pressure pillow commence recording automatically the mass increase within the trap. To be able to analyse the trapped material a crane withdraws the filled container and places it on to the riverbank. The empty trap has to be reinserted into the riverbed for further measurements.

Bedload traps enable continuous and automatic bedload transport measurements and achieve accurate and reliable results. Thereby, the method is applicable for all water stages, especially during floods, when other sampling methods are not operable anymore. Besides, it enables the determination of the complete grain size spectrum. The sampling durations depend on the intensity of bedload transport and is limited by the reservoir capacity of the trap. The measured mass increase by time enables the calculation of the specific bedload transport and further provides an excellent inside in the temporal variability of bedload transport process. Due to its fixed position in the cross-section, the gathered information is spatially limited. This limitation can be reduced by additional measurements with surrogate instruments like plate geophones. Bedload traps are well suited to calibrate the signal of surrogate instruments (geophone impulses).

In situ and laboratory measurements have revealed that the trap has a high hydraulic efficiency. Habersack et al. (2001) have shown for a slot trap applied in the Drau River, that the hydraulic efficiency is almost one until a filling stage of 80 percent of the trap volume.

Figure 11 Maintenance work on bedload traps, Dellach / Drau (Aigner, 2012)

Figure 12 removal of the sampling box, Maria Alm / Urslau (Kreisler, 2012)

Figure 13 bedload monitoring station with bedload trap, Moulin catchment

2.3 Monitored Retention Basin

Bedload monitoring stations built with a retention basin basically operates as a big trap able to retain all the sediment transported by a stream. Very few experimental monitoring stations of this kind are currently active in the Alps (Rio Cordon in the Italian Alps and Erlenbach in Swiss Alps) due to their high building costs and as well as the effort for their maintenance However, in the past, more stations have been realized in the Italian Alps (e.g. Missiaga and Rio Gallina creeks).

Such stations can provide data on single events' sediment volumes if these are surveyed only occasionally, i.e. after the occurrence of sediment transporting flows, or continuous bedload data (in conjunction with water discharge and possibly suspended transport concentration) when a direct system for measuring bedload transport rates is implemented.

The Rio Cordon station, built in 1986 and managed by ARPAV (Veneto Region), works with the basic principle to record the separated accumulations of coarse and fine sediment over time by means of ultrasonic sensors (for the former) and pressure cells (for the latter). In order to do this, the Rio Cordon station is equipped with an inclined grid (2 cm spacing) where the separation between coarse and fine sediments takes place, with a dry storage area for coarse sediment deposition a set of ultrasonic sensors to ensures a detailed recording of the deposited volume accumulation during a flood event and a pool where the sediment (and water) passing through the grid is deposited, monitored by pressure cells (Figure 14 and Figure 15).

Suspended sediment concentration – beside water discharge – is also measured at the station. For a detailed discussion of pros and cons of the Rio Cordon station, as well as for a summary of the insights gained from its operation, see Mao et al (2010).

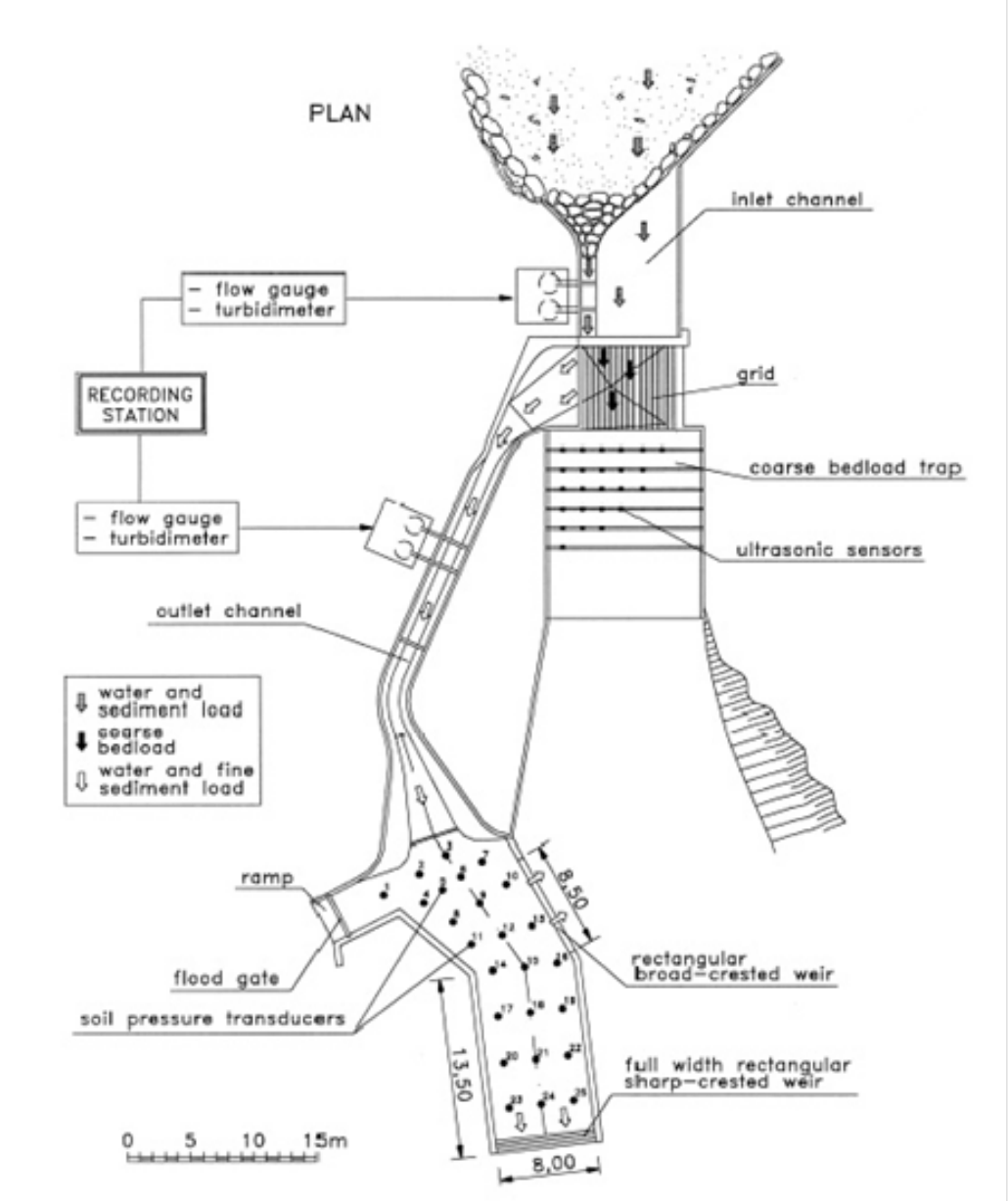

Figure 14 Plan view of the Cordon stream sediment measuring station provided with retention basins

Figure 15 Views of the Cordon stream measuring station: a) Downstream view of the bedload storage, the outlet flume and the two buildings hosting instrumentations and the emergency power system; b) Upstream view of the fine sediment settling basin; c) Downstream view of the separating grid, the bedload storage area and the cable frame which host the 24 ultrasonic sensors; d) Upstream view of the bedload storage area and the ultrasonic sensors; e) Downstream view of the inlet channel; f) Downstream view of the outlet channel with the Partech SDM-10 light absorption turbidimeter fixed under the bridge (from Mao et al., 2010)

Simpler instrumentations and temporally-coarser volume assessment (event scale) were deployed in the Missiaga and Gallina retention basins.

The experimental basins along the Valle della Gallina (North-western Italian Alps) is promoted and managed by CNR-IRPI, branch of Turin; the main stream is under observation since 1982 and is equipped with one in-channel natural debris pool regularized into the bottom bedrock, in order to measure the delivered sediment volumes (Figure 16 a and b) (Maraga et al., 2011).

Figure 16 a - Gallina Valley monitoring station, managed by CNR – IRPI of Turin: sediment trapped volume in the debris pool; b - The sedimentary station during material removal and measurement (from www.irpi.to.cnr.it)

The Missiaga catchment, located in the Dolomites (North-eastern Italian Alps), was studied by the CNR-IRPI of Padua from 1982 to 2001. A discharge gauge station was installed, in correspondence of an existing check and behind it a natural retention basin allowed the accumulation of the sediment bedload (Figure 17). After flood events with notable sediment transport, the stored volume was evaluated by topographic surveys of some fixed sections and then removed (Villi et al., 1985; Anselmo et al., 1989).

Figure 17 Missiaga stream monitoring station, managed by CNR – IRPI of Padua: discharge gauge station, active from 1983 to 2001, in correspondence on an existing check dam, and upstream retention basin. System now dismantled

Mao et al (2009) analysed together bedload data from the Rio Cordon, Missiaga and Gallina stations.

The Erlenbach catchment is located in the Alptal valley in the Pre-alps of central Switzerland (Hegg et al., 2006); in order to measure the total amount of sediment transported by the Erlenbach, a sediment retention basin with a capacity of about 2000 m^3 was built in 1982 just downstream of the gauging station and actually managed by WSL (Figure 18) (Rickenmann et al., 2012). The bedload volume accumulated in the retention basin was measured using a graduated rod from a boat and since 2006, with a tachymeter or a terrestrial laser scanner (TLS), after the water is drained through the bottom outlet from the basin.

The measurement facility was enhanced by direct measurements made with: PBIS (piezoelectric bedload impact sensor), geophones and an innovative and unique moving basket system (Rickenmann et al., 2012; Figure 19). The basket system permit to obtain bedload samples over short sampling periods, measure the grain size distribution of the transported material and its variation over time and with discharge, obtain direct bedload measurements and improve the geophone calibration. For a more detailed discussion of the Erlenbach station see Rickenmann et al (2012).

Figure 18 Retention basin of the Erlenbach, managed by WSL (from www.wsl.ch)

Figure 19 Erlenbach catchment: overview of automated basket sampler system and the retention basin (from www.wsl.ch)

2.4 Geophone plates

Geophone plates are a qualitative, indirect method for monitoring bedload transport. Geophones have its origin in seismic subsurface exploration and are basically constructed to detect vibrations.

For bedload monitoring, geophones are typically mounted on 15 mm x 360 mm x 500 mm big steel plates (Figure 20). The geophone devices (Figure 21) are installed bed parallel over a whole cross section of a river or torrent (Figure 22). During bedload transport, gravel moves over the steel plates and creates impact shocks. These vibrations are detected by the geophone. An analyzing software processes the raw data signal continuously and automatically. To reduce the immense amount of data, following parameters are computed and stored: impulses per minute (threshold value of 0.1 V), maximum amplitude per minute and cumulative integrals of the signal (Habersack et al., 2012). Geophone impulses are highly correlating with bedload transport for grain sizes D>20 mm (Rickenmann et.al, in prep.). For special purposes (e.g. parallel to direct bedload transport measurements) recording of parameters per seconds or raw data recording is possible.

Geophone data, which is high in spatial and temporal resolution, provides permanent information about the distribution and intensity of bedload transport within the whole cross-section of a river. The geophone device enables continuous measurement even during high flow conditions.

Figure 20 Geophone mounted on a steel plate (Seitz, 2007)

Figure 21 Geophone device (Seitz, 2007)

Figure 22 Geophon Installation Lienz/Drau (Aigner, 2011)

Following Parameters of the 10 kHz sensor signal are computed for every geophone:

impulses per minute [Imp] - whenever the geophone signal exceeds a threshold value of 0.1 V, an impulse is recorded. Cumulative value

maximum amplitude per minute [V]

quadratic integral per minute [V² s] – sum of the squared amplitude values multiplied by 0.0001 seconds (based on sampling rate of 10 kHz). Cumulative value

Calibration of plate geophone systems is needed and can be reached with direct bedload transport measurements. Generally geophone impulses show a high correlation with bedload transport mass at a given site (e.g. Rickenmann et.al, in prep.). Therefore, a calibrated plate geophone system allows the calculation of bedload transport rates and yields.

Overall, plate geophone systems are an appropriate monitoring device to collect a wide spectrum of information about bedload transport. The recorded geophone data can be used for analyzing:

- temporal variability of bedload transport (Figure 23)
- spatial variability of bedload transport (Figure 23)
- initiation of bedload transport (initiation of motion)
- bedload transport processes (e.g. amour layer effects, bedload input from tributaries,..)
- calculation of bedload transport rates and yields (if geophones are calibrated)

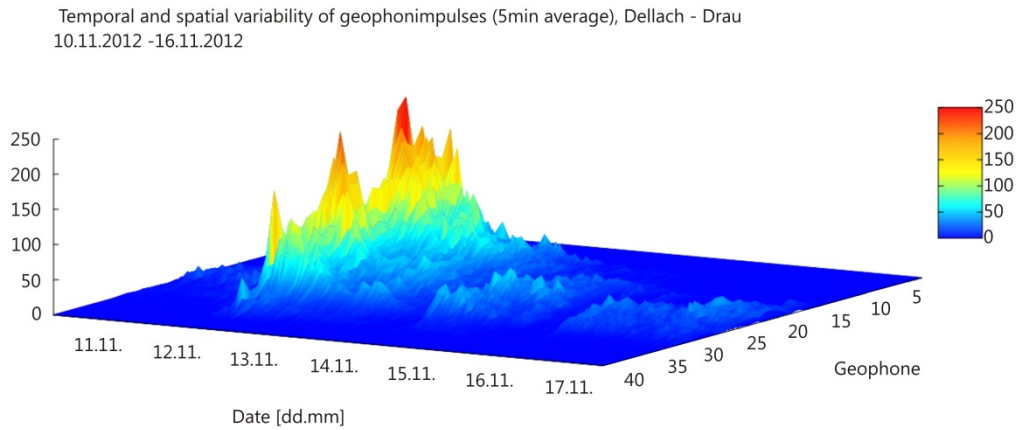

Figure 23 temporal and spatial variability of bedload transport, data collected with bedload plate geophones, Dellach / Drau (Aigner, 2012)

2.5 Japanese Pipe Hydrophone (Acoustic pipe sensor)

The “pipe hydrophone” or “pipe geophone” (as named by his developers, Mizuyama et al., 2003) is a steel, air-filled pipe with a microphone inside which detects the acoustic vibrations induced by hitting particles. As it is not really either a hydrophone (i.e. it does not record the vibrations transmitted in the water medium) or a geophone (i.e. it does not record velocities of ground vibrations) a more adequate name is probably “acoustic pipe sensor”.

Vibrations induced by moving particles hitting the pipe are amplified by a pre-amplifier and then transmitted to a converter, which, whenever a certain threshold is passed, generates a voltage processed through a 6-channel band-path filter, where each channel features a gain of 4 relative to the previous channel (Mizuyama et al., 2010b, Figure 24).

Figure 24 The acoustic pipe sensor (“pipe hydrophone” or “pipe geophone”) manufactured by Hydrotech Company (Japan). The half-buried pipe (a), the microphone inside (b), the preamplifier (c), and the converted (d). From Mizuyama et al. (2010b).

The converter signal is processed by a 8-channel interval timer attached to a data logger – both of them installed in a case on the river bank, where a solar panel and a battery supply the required power to the system. Impulses for each channel are recorded by the data logger at 1 min interval.

Acoustic pipe sensors were originally developed and installed to integrate bedload motion (collisions) and thus transport rates (after calibration) through a stream cross-section, without information on the cross-wise variability in transport. However, if several short pipes are deployed across a section, such spatial variability can be detected similarly (but not to the same extent) to geophone plates.

Pipe sensors installed in Japan vary in length, from 0.3 m to several meters (as in Figure 24), but the shorter the pipe the easier is the calibration in the field by means of direct methods (traps or samplers). Factors influencing the calibration of the acoustic pipe have been investigated also in the lab (Mizuyama et al., 2010a). As for geophone plates, acoustic pipe require a stable cross-section (no erosion but also no aggradation) for their installation, and thus check-dams' crest provide the best option in many mountain rivers (as in Figure 24). Acoustic pipes have proven robust enough to be deployed in rivers featuring transport of large cobbles and smal-sized boulders.

As remarked by Mizuyama et al. (2010b), the performance of this system is acceptable for low bedload discharges as long as pulses are integrated over sufficiently long intervals and anyhow for grain sizes > 4 mm. The performance is better for intermediate bedload rates, but for high bedload fluxes (as during floods) the outputs from the different channels have to be compared to ensure that signal damping does not occur. Finally, it is important to point out that the calibration relationship of acoustic pipes appears to be quite site-dependent and moreover susceptible to variations over time of the geometrical and hydraulic characteristics of the pipe-crest aera (e.g. due to concrete wearing).

2.6 Tracers

Sediment tracing represents an important methodology for bedload transport analysis, and over the last 50 years has led to significant advances in the understanding of the stochastic nature of bedload motion in gravel- and cobble-bed rivers. A bedload tracer is a sediment clast (from gravel to boulder size) made recognizable from the others - by different

methods as it will be explained below - which is followed in its displacement at different times and/or at different locations along the river channel.
In particular, the use of tracers is highly valuable for the quantification of motion thresholds conditions (e.g. Wilcock, 1997; Lenzi et al., 2006) and travel distances (e.g., Hassan and Church, 1992; Lièbault et al., 2012) as a function of particle grain size and reach characteristics. Also, combined with scour chains (see Section 2.7.4), they provide a means for assessing time-integrated bedload transport rates (Haschenburger and Church, 1998; Wong et al., 2007; Liébault and Laronne, 2008).
The first field studies deploying tracers in river channels date back to the 1960s, with the use of painted tracers. Despite its simplicity, the use of painted particles whose positions is surveyed at different times – in particular before and after each competent flow – is still a valid tool especially in rivers where burial probability is low (e.g. Mao and Surian, 2010). However, in studies with low recovery rates (in some cases < 30%) the statistical properties of travel distances may not be representative of actual bedload dispersion (Lièbault et al., 2012).

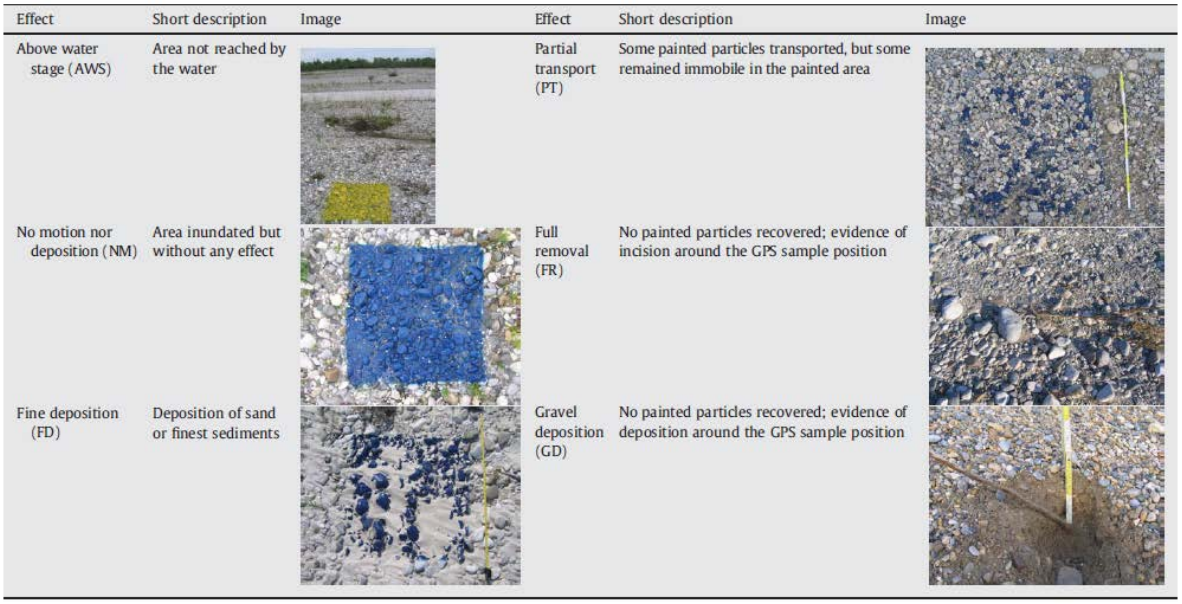

Figure 25 Use of painted clasts in the Tagliamento River (from Mao and Surian, 2010)

More sophisticated tracers – magnetic, radiotransmitters and electromagnetic – detectable also when buried have been developed and deployed during the last 20 years, leading to higher quality data (see Hassan and Ergenzinger, 2003; Habersack, 2001; Liedermann et al., 2013). In particular, since the 2000s, RFID (i.e. radiofrequency identification) tagging technology - initially applied in commercial environmental research to animal tracking - has become very common to

track sediment particles in gravel- and cobble-bed rivers. RFID technology uses electromagnetic coupling to transmit an identifi cation code as 'noise' on a radio frequency signal. This code is unique to each tag, while the transmission frequency is shared.

RFID tagging includes both, active and passive system. The former have their own battery (but at the moment with a duration limited to a few years), are relatively large (several centimeters in length) and quite expensive, but could potentially permit the detection of the tagged particles from relatively long distances (i.e. from river banks). In contrast, passive integrated transponders (PITs) are smaller (down to about 1 cm in length, few mm in diameter), long-lasting and cheap. However, their detection range is of the order of 0.5-1m (but depends on both PIT length and antenna diameter) as they do not have a battery and the antenna is the source of energy for them to send out their signal. For a recent review of tagging methods, the paper by MacVicar et al. (2011) is quite useful even though addresses specifically wood transport monitoring.

PITs have been deployed in a variety of fluvial environments for bedload tracing. Early studies (Nichols, 2004; Lamarre et al., 2005) conducted in small streams gave recovery rates above 85%, whereas more recent studies in large gravel-bed rivers obtained lower recovery rates (Camenen et al., 2010; Lièbault et al., 2012). The lower recovery rates in larger and more mobile streams stem from the higher probability of tagged clasts burial by sediment lobes as well as by longer travel distances once tracers move in the main channel.

PIT-tagged particles are either created by "molding" the clast itself around the transponders (Nichols, 2004) or by drilling a hole – in the lab or directly in the field – in natural clasts of different size (the minimum grain diameter is limited by PIT size and clast resistance) and then fixing with epoxy glue the PIT inside it (Lamarre et al., 2005; Lièbault et al., 2012). Once ready, PIT-tagged clasts are released in the river bed at different sections, possibly spanning different morphological units.

Most typically, after a flow event potentially capable to transport the tagged clasts, their search is carried out locating them by a mobile antenna deployed by an operator scanning the river channel, preferably at low flows in wadable streams (Figure 20). Tagged clast location is then registered either by GPS or by traditional survey methods (range finder or total station plus stakes on banks). The travel distance of each clast is then computed from simple topographic calculations, and its virtual velocity (i.e. including resting times between motions) can also be determined when the travel time is estimated from an analysis of flow hydrographs (Haschenburger and Church, 1998). As mentioned above, coupling this

information with scour depth leads to an assessment of integrated bedload transport rates (see Section 2.7).

Figure 26 Searching PIT-tagged clasts by a mobile antenna in the Strimm creek (Italy)

More recently, stationary antennas stretched across the river bed (either buried within or suspended over the bed, Figure 26) have been installed in mountain rivers to detect the exact time (at 1s resolution) of tracers passage (Dell'Agnese et al., 2012). The use of multiple antennas along a river reach permit a much more reliable determination of clasts' virtual velocity, along with an accurate assessment of incipient motion conditions when tagged clasts are placed in the near proximity of antennas. Of course, the highest information from PIT tags can be obtained combining stationary and mobile antennas in the same river reach.

Figure 27 Stationary antennas in the Saldur River (Italy), installation of a buried antenna (later anchored by large rocks);

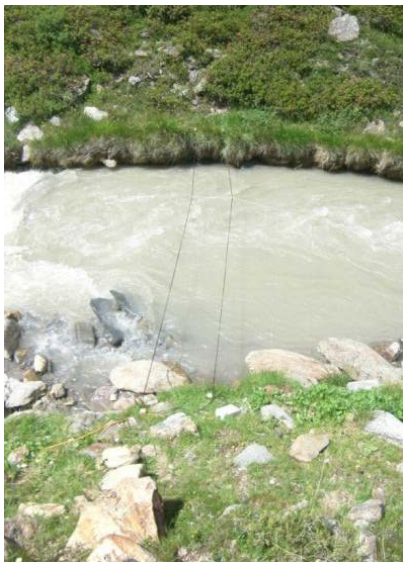

Figure 28 Stationary antennas in the Saldur River (Italy), a suspended antenna.

2.7 Topographic / morphological methods

Topographic methods are addressed here as methods that allow for a quantification of sediment budgets for river (and associated floodplain) reaches through repeated, using traditional (scour chains, levelling of cross and longitudinal profiles and surveys using total stations) and modern techniques (differential GNSS, LiDAR, UAV-based stereophotogrammetry). The latter group of methods enables the generation of high-resolution digital elevation models (DEMs); by calculating the local differences in two DEMs representing the surface, e.g. of a gravel bar, at different points in time, changes in surface elevation and in volume (scour-and-fill analysis) can be quantified. Therefore, these methods do not measure or monitor bedload transport rates but rather the changes in surface elevations and sediment storage caused by the latter over time. Sections 2.7.1-2.7.3 focuses on the generation and morphometric analysis of DEMs generated from LiDAR surveys and photogrammetry.

2.7.1 Terrestrial Laser scanning

2.7.1.1 Introduction

Laser scanners are capable of surveying between 10^3 and 106 points per second from an airborne (airborne laser scanning, ALS) or fixed/tripod-mounted (terrestrial laser scanning, TLS) platform. ALS accuracies are in the range of several centimetres in location and in the order of 10-20 cm in elevation (see e.g. Scheidl et al., 2008 and Hodgson and Bresnahan, 2004). The comparatively large uncertainty is compensated, for most applications, by the large areal coverage of ALS surveys. TLS surveys generate very high point densities (10^2-10^3 points per square meter), and their accuracy is higher (in the order of several few cm in elevation, see e.g. Schürch et al., 2011); their areal coverage, however, is limited, unless multiple surveying stations or mobile platforms (cars, rail vehicles or boats, c.f. Hohenthal et al., 2011) are used; as ALS surveys are by far more expensive in terms of time and cost, TLS lends itself much better for local-scale monitoring tasks, at a temporal resolution that is only limited by the time required for setting up the scanner (at multiple stations if need be) and the acquisition time. Modern terrestrial laserscanners can survey surfaces in several 10^2 up to 10^3 meters of distance; the beam diameter on the target (“footprint”), however, increases at larger distances, which negatively affects spatial resolution and data quality; therefore, depending on the device, the distance between the station and the surfaces to be surveyed should be kept as small as possible (e.g. 100-200 m).

In geomorphology, the emergence of LiDAR applications led to the generation and analysis of DEMs of previously unknown spatial resolution. A recent paper by Hohenthal et al. (2011) reviews laser scanning applications in fluvial studies. For sediment management, LiDAR applications can be categorised in two groups:

- First, the morphometric analysis of single DEMs on several spatial scales, for example the characterisation of substrate properties, roughness and on the plot and reach scale (Brasington et al., 2012, Hodge et al., 2009), and the characterisation of bedforms (Cavalli et al., 2008).
- Second, the repeated acquisition of digital surface data and the comparison of land surfaces surveyed at different points in time. In fluvial geomorphology, TLS can be used to monitor morphodynamics on submeter to kilometre spatial scale, with a (sub-)daily to (multi-)annual temporal resolution (Heritage and Hetherington, 2005, Milan et al., 2007, Heritage and Hetherington, 2007, Schürch et al., 2011). Heritage and Hetherington (2007) provide a comparison of field survey techniques with respect to accuracy and point spacing.

In the following paragraphs, we concentrate on the application of TLS for morphometric and monitoring studies in fluvial environments, specifically for the quantification of changes in sediment storage (which is related to bedload transfer and sediment budgets). We describe the setup of the device, and the evaluation of results. The calculation of sediment budgets from multitemporal DEMs is described in section 2.7.3.

2.7.1.2 Field site preparation and station set-up

Multitemporal TLS surveys of a field site have to be carefully planned. Depending on the complexity of the surface, and the size and geometry of the unobstructed viewshed, one to several stations for the scanner have to be located. Several stations are recommended to avoid shadowing (causing “no data” patches in the resulting datasets), to optimise point densities within the area of interest, and to warrant favourable acquisition geometry. Flat angles of beam incidence should be avoided; hence, in a fluvial environment, elevated stations (e.g. on a terrace, on a neighbouring hillslope) should be given preference over stations on the floodplain. Heritage et al. (2009) give recommendations on the survey strategy in fluvial settings.

During data processing, the overlapping point clouds from several scanner stations have to be combined to form a single point covering the whole area of interest. Notwithstanding software tools to co-register point clouds

acquired from multiple stations using iterative algorithms (Schürch et al., 2011 report errors for point cloud matching between 2.9 and 6.1 cm), we recommend the installation of fixed reflector targets on stable objects or surfaces more or less evenly (i.e. across different distances, angles and elevations) across the area of interest. These are necessary as tie-points to facilitate, through resection, the accurate setup of the measurement device for future surveys, to accurately co-register point clouds from multiple stations, and to provide real-world coordinates for the point clouds.

The timing of a TLS survey is important in fluvial environments: Current TLS devices frequently use near infrared lasers the pulses of which are absorbed by water; hence, submerged portions of the area of interest cannot be surveyed. Low water levels at the time of survey maximise the areal coverage of LiDAR data (Milan et al., 2007). The application of green wavelength lasers to bathymetric applications in fluvial settings is presently developing (Williams et al., 2012); where such devices are not available, immersed topography has to be surveyed with different methods (e.g. levelling of cross-profiles using total stations, surveying of the bedforms of wadeable channels using differential GNSS.

2.7.1.3 Preprocessing of data and DEM generation

The collected raw data are processed using (device-specific or generic) software packages for registration, blending and colouration of the point clouds. This includes manual and (semi-)automatic iterative filtering procedures to remove blunders (e.g. “flying points” caused by birds, insects etc) and to filter the point cloud in order to remove vegetation, making the initial DSM (digital surface model) a DTM (digital terrain model)(Meng et al., 2010, Sharma et al., 2010, Coveney and Stewart Fotheringham, 2011). Manual work on the point cloud can be a tedious procedure, but can hardly ever be avoided. For many applications, the point data will be converted to a raster format, which requires the use of gridding and interpolation algorithms, the choice of which affects the quality of the resulting raster DEM (Heritage et al., 2009, Bater and Coops, 2009, Erdogan, 2009).

2.7.2 Drone-based aerial imagery

Another recently emerging technology is the acquisition of digital aerial imagery from remote controlled unmanned aerial vehicles (UAV), or drones (Mirijovsky, 2012, Hugenholtz et al., 2013). UAVs allow repeat surveys at small temporal scales and offer independence from the time frame of

official aerial survey campaigns. They exist in several designs; multicopters, for example, can stand still while airborne and are easily navigated manually, but are more suitable for small areas and complex conditions (e.g. starts and landings in forest clearings). Contrary, fast-moving model aircraft rely on GNSS-controlled autopilot systems and are capable of covering larger areas. So-called blimps and other tethered aerial vehicles offer an alternative for image acquisition on the local scale (Vericat et al., 2009).

For a successful image acquisition, ground-control targets (e.g. wooden or metal crosses painted with prominent colours, reflective targets on top of coloured foil patches) surveyed with differential GNSS are placed in the field, enabling the alignment of overlapping images and the ortho-rectification procedure. GNSS-controlled UAVs allow for the planning of flight paths tailored to the area of interest and the required degree of overlap between images.

After stereophotogrammetric analysis in specialised software packages, orthophotos and DEMs of very high resolution (for orthophotos, the resolution can be in the order of only few centimetres per pixel) are generated, even if the camera has not been calibrated (through the application of “structure-from-motion”, Westoby et al., 2012). The resulting orthophotos can be used for multitemporal mapping of channel planform change, the development of sediment storage, riparian landuse and vegetation, surface granulometry etc (e.g. Morche et al., 2008). Fonstad et al. (2013) report that the precision of UAV-based DEMs is comparable with ALS; similarly, their acquisition geometry makes them highly suitable for flat and moderately steep (but not near-vertical) terrain. Unlike ALS, where the laser beam occasionally reaches the ground even through dense vegetation canopies, the “virtual removal” of vegetation from stereophotogrammetric drone-based DEMs is hardly feasible. Therefore, the application of this technology appears to be currently restricted to unvegetated portions of study areas.

2.7.3 Morphological sediment budgets from multitemporal digital elevation models

General remarks:

DEMs of difference (DoDs) generated from the cell-by-cell subtraction of two DEMs allow for the quantification of the magnitude and spatial distribution of surface changes between two surveys (James et al., 2012) and can also be used to quantify volumes of deposition and erosion (“scour-and-fill” analysis, e.g. Haas et al., 2012). In scour-and-fill analyses

based on raster DEMs, local differences in elevation [m] can be converted to eroded or deposited volume by multiplying with the raster cell size [m²]. Monitoring studies will mostly rely on repeat TLS studies, for reasons explained earlier, but there is also some potential in combining pre-event ALS-based DEMs and TLS surveys conducted after an event (Bremer and Sass, 2012). The former data are widely available, while the second are comparatively inexpensive and can be quickly arranged as occasion offers.

For the balancing of erosion and deposition within river reaches, Lindsay and Ashmore (2002) describe the effect of survey frequency; they conclude that longer intervals between measurement cause a (negative) bias for scour, fill, and net balances, because erosion and deposition tend to compensate each other on longer time scales. This should be kept in mind when using multitemporal DEMs for the assessment of bedload transfer.

Error assessment:

For an error assessment of scour-and-fill analyses, two options are given here:

- Repeat scans of a part of the area of interest conducted on the same date (and hence containing two point clouds from in fact unchanged terrain) allow for an error assessment of a single DEM. A DoD of the two DEMs is produced, the arithmetic mean (which should be zero) and the standard deviation σ_{DEM} are calculated, and the latter is used as a measure of uncertainty for a single DEM. For the error assessment of i) changes in surface elevation and ii) the eroded/deposited sediment volume, the uncertainty of each single DEM is propagated to the respective result (Lane et al., 2003). From the resulting σ_{DoD}, a "level of detection" (LoD) can be derived using probabilistic theory (e.g. LoD = $2\sigma_{DoD}$), and differences below that threshold are set to "no change". The uncertainty can also be propagated to volume calculations, as advocated by Lane et al. (2003).
- The uncertainty of the DoD can be assessed directly using a part of the DoD representing a stable, unchanged area. The latter has to be identified on the grounds of local or expert knowledge; the choice of stable areas is facilitated by simultaneously taken digital images. Within the stable area, , σ_{DoD} is the standard deviation of the DoD (one should also check the mean for a potential bias if the mean is different from zero).

For more detailed studies on uncertainty in the detection and quantification of surface changes, the reader is referred to Lane et al. (2003), Wheaton et al. (2010), and Schürch et al. (2011).

2.7.4 Scour chains

Scour chains can be used simultaneously with tracers to assess the time-integrated bedload yield passing through an alluvial river reach (Laronne et al., 1992; Haschenburger and Church, 1998; Liébault and Laronne, 2008). It is based on the continuity equation for sediment, which is simplified to obtain the event-based bedload transport volume from the dimensions of the active layer of the bed and the mean distance of transport of individual particles:

$$V_b = (d_b * w_b * L_b) * (1-p) \qquad (1)$$

where V_b (m3) is the total volume of bedload transported during a flow event, d_b (m) is the active depth of the bed, w_b (m) is the active width of the bed, L_b (m) is the arithmetic mean travel distance of moving particles and p is sediment porosity.

The active depth of the bed, d_b, is defined as the overall magnitude of vertical bed level oscillations that occur during a flow event as a result of processes of scour and fill. It is computed as the arithmetic mean of the absolute magnitudes of scour and fill depths recorded by monitoring tools. Several field devices may be used to measure depth of scour and fill, of which scour chains are the most common (Laronne et al., 1994); they record for each sampling point the event-based maximum depth of scour and the net deposition (Figure 29). The active width of the bed, w_b, is the cross sectional span where vertical bedload oscillations are observed. The active width of the bed may be determined by inserting scour and fill devices at small, regular intervals across the channel bed.

Figure 29 an example of scour chain buried after a flow event on the Moulin Ravine, Southern French Alps

The mean travel distance of moving particles is determined by insertion and relocation of tracers that are similar in size, shape and density to sediment in the channel reach. A range of tracing techniques has been deployed in various environments (Sear et al., 2000) and specifically in gravel-bed rivers (Hassan and Ergenzinger, 2003). The most common are painting, magnetic tracing, and more recently PIT tags (Lamarre et al., 2005; Liébault et al., 2012).

Sediment porosity may be estimated from the grain size distribution of the subsurface (Carling and Reader, 1982) or determined directly in the field by measuring the volume of water that displaces a weighed sediment sample representing the active layer. A detailed description of the field procedure is available (Bunte and Abt, 2001).

As for other morphological approaches, the chain and tracer method is relevant when bedload transport is supplied by in-channel sediment stores. It is not applicable when bedload moves on a fixed river bed (e.g., reaches comprised of bed material inherited from a past sediment regime).

3 Suitability of bedload monitoring methods

In Table 2 are listed the suggested acquisition parameters for the main devices commonly applied for bedload monitoring.

Table 2 Suggested acquisition parameters for different instruments used in bedload monitoring

Instrument type	Variable to monitor	Recording intervals / spatial resolution	Other parameters / note
Basket sampler: cross section-wise measurement	- total bedload rate - bedload volume	20 sec – 1 h* *long durations preferable at low and moderate transport rates, shorter (5-10 min with Bunte traps) at high transport rates	Sampler characteristics types (intake width, mesh size) depending on transported grain size and flow depth/velocity
Basket sampler: repeated measurement	- variation over time of specific bedload rate at selected sites -incipient motion conditions	20 sec – 5 min	Sampler characteristics types (intake width, mesh size) depending on transported grain size and flow depth/velocity
Slot trap	- specific bedload rates	5 min – 24 h	Trap volume to be designed based on floods duration/expected bedload rates Trap opening to be designed based on transported grain size
Monitored Retention Basin	- bedload yield during single events (total bedload rate if accumulation continuously monitored)	1- 5 min (for obtaining bedload rates) Before and after flood event (for bedload volumes)	See for example: - Erlenbach (CH) - Rio Cordon (I)

Geophones Plates	intensity of bedload transport (impulses, amplitudes, integrals)	1 min (resolution of 1 sec and raw data possible)	Sampling rate 10 kHz Common threshold for impulses =0.1 V
Acoustic pipe sensor (Japanese pipe hydrophone)	intensity of bedload transport (number of pulses/particle collision per unit of time)	1 min	Calibration potentially better when integrated over longer time intervals (5-10 min)
Tracers	- incipient motion conditions - travel distance - virtual clast velocity - velocity - transport path	- by mobile antennas: re-survey of tracers after each potential transporting event - by stationary antennas: 1 sec passage records	Tracers most effective in wadable relatively narrow streams (characterized by low transport rates) but also useable in non-wadable rivers
Terrestrial Laser scanning	variation in sediment storage	Survey frequency: Hours if necessary, typically days to months; spatial resolution: <5-10 cm	Restrictions apply when visibility is low (e.g. forested terrain), submerged topography cannot be surveyed
Drone-based aerial imagery	variation in sediment storage, river planform change	Survey frequency: Hours if necessary, typically days to months; spatial resolution: 5-10 cm	Restrictions apply when visibility is low (e.g. forested terrain), submerged topography cannot be surveyed
Scour chains	-erosion/Deposition -variation in sediment storage		

Table 3 presents a classification in terms of suitability of bedload monitoring devices concerning specific parameters (modified from Habersack et al., 2010). The point classification is as follows:

●●● highly suited for measuring this parameter

●● suited for measuring this parameter

● partially suited for measuring this parameter

not suited for measuring this parameter

Table 3 Suitability of bedload monitoring devices concerning specific parameters (modified from Habersack et al., 2010)

Parameters of Interest	Basket Sampler (cross section wise)	Basket Sampler (repeated)	Bunte traps (for wadable streams)	Slot Trap	Monitored Retention Basin	Geo-phones	Acoustic pipe sensor	Tracers	Terrest-rial Laser scanning	Aerial imagery	Scour chains
Specific bedload rate *[kg m^{-1}s^{-1}]*	●●●	●●●	●●●	●●●	●●	●	●				
Bedload rate *[kg s^{-1}]*	●●●		●●●	●	●●	●	●	●			
Total bedload volume *[kg]*	●●●		●●●	●	●●●	●	●	●			
Spatial variability of bedload discharge	●		●●●		●	●●●	●	●●			
Temporal variability of bedload discharge	●	●●●	●	●●	●●	●●●	●●●				
Initiation of motion *[m; m^{3}s^{-1}]*	●	●●●	●●	●●●	●●●	●●●	●●●	●●●			
Transport path/ velocity *[m; m s^{-1}]*					●●●			●●●			
Variation of sediment storage									●●	●●	●●

4 Field forms - Bedload Monitoring

4.1 Specific Field form

4.1.1 Specific Field form - Basket Sampler (interval measurement)

Field form - Bedload Measurement						
Method: mobile basket sampler			**Measurement procedure: repeated / intervall**			
Monitoring device:			Mesh size [mm]:			Intake [mm]:
Date:			Person:			Time:
Project:			River:			Country:
Region:			Station:			Remarks:
Discharge [m^3s^{-1}]:			Water temperature [°C]:			
Waterlevel [m]:			Turbidity [mg l^{-1}]:			
Identification	Location in the cross-section	Start of measurement [hh:mm:ss]	End of measurement [hh:mm:ss]	Duration [sec]	Waterlevel [m]	Remarks
M1-L1	L1	15:25:00	15:26:00	60	1.57	
M2-L1	L1	15:42:00	15:45:00	180	1.57	
M3-L1	L1	15:48:20	15:51:20	180	1.58	
M4-L1	L1	16:01:00	16:03:00	120	1.57	

4.1.2 Specific Field form - Basket Sampler (cross-section wise measurement)

Field form - Bedload Measurement						
Method: mobile basket sampler			**Measurement procedure: cross-section wise**			
Monitoring device:			Mesh size [mm]:			Intake [mm]:
Date:			Person:			Time:
Project:			River:			Country:
Region:			Station:			Remarks:
Discharge [m^3s^{-1}]:			Water temperature [°C]:			
Waterlevel [m]:			Turbidity [mg l^{-1}]:			
Identification	Location in the cross-section	Start of measurement [hh:mm:ss]	End of measurement [hh:mm:ss]	Duration [sec]	Waterlevel [m]	Remarks
M1-L1	L1	15:25:00	15:26:00	60	1.57	
M2-L1	L1	15:42:00	15:45:00	180	1.57	
M3-L1	L1	15:48:20	15:51:20	180	1.58	
M4-L2	L2	16:01:00	16:03:00	120	1.57	
M5-L2	L2	16:09:00	16:11:00	120	2	
M6-L2	L2	16:16:00	16:18:00	120	2	
M7-L3	L3	16:24:00	16:26:00	120	2	

4.1.3 Specific Field form – Bedload Trap

Field form - Bedload Measurement					
Method: bedload trap					
Monitoring device:			Sampling volume [m³]:		Slot width [mm]:
Date:			Person:		Time:
Project:			River:		Country:
Region:			Station:		Remarks:
Discharge [m^3s^{-1}]:			Water temperature [°C]:		
Waterlevel [m]:			Turbidity [mg l^{-1}]:		
Identification	Time [hh:mm:ss]	Trap weight [kg]	Waterlevel [m]	Additional data	Remarks
Dellach 2013 Trap 1 - 1	15:25:00	3	1.57		trap open
	15:42:00	17	1.57		
	15:48:20	34	1.58		
	16:01:00	65	1.57		
	16:12:00	88	1.58		
	16:23:00	142	1.62		

5 References

Anselmo V., Marchi L., Tecca P.R., Villi V. (1989). Sediment transport in a small watershed of Dolomite Mountains (NE Italy). Quaderni di Idronomia Montana, 9, pp. 69-81

Bater, C.W., Coops, N.C., 2009. Evaluating error associated with lidar-derived DEM interpolation. Computers & Geosciences 35, 289-300.

Bänziger R., Burch H. 1990. Acoustic sensors as indicators for bed load transport in a mountain torrent. In Hydrology in Mountainous Regions I, Lang H, Musy A (eds), IAHS Publication no. 193. IAHS:Wallingford; 207–214.

Brasington, J., Vericat, D., Rychkov, I., 2012. Modeling river bed morphology, roughness, and surface sedimentology using high resolution terrestrial laser scanning. Water Resour. Res. 48, W11519.

Bremer, M., Sass, O., 2012. Combining airborne and terrestrial laser scanning for quantifying erosion and deposition by a debris flow event. Geomorphology 138, 49-60.

Bunte K, Abt SR, 2001. Sampling surface and subsurface particle-size distributions in wadable gravel- and cobble-bed streams for analyses of sediment transport, hydraulics, and streambed monitoring. RMRS-GTR-74, USDA Forest Service, Rocky Mountains Research Station, General Technical Report 74.

Bunte K., Abt S.R., Potyondy J.P., Ryan S. (2004): Measurement of coarse Gravel and cobble Transport Using Protable Bedload Traps, Journal of Hydraulic Engineering, Vol. 130, No. 9, pp. 879-893.

Bunte, K., K. Swingle, and S.R. Abt, 2007. Guidelines for using bedload traps in coarse-bedded mountain streams: Construction, installation, operation and sample processing. General Technical Report RMRS-GTR-191, Fort Collins, CO, U.S. Department of Agriculture, Forest Service, Rocky Mountain Research Station, 91 pp. http://www.fs.fed.us/rm/pubs/rmrs_gtr191.pdf.

Bunte, K., Abt, S.R., Potyondy, J.P., and Swingle, K.W. 2008. Acomparison of coarse bedload transport measured with bedload traps and Helley-Smith samplers. Geodinamica Acta 21: 53–66.

Bunte, K., Abt, S.R., Swingle, K.W., and Potyondy, J.P. 2010. Bankfull mobile particle size and its predictions from a Shields-type approach. Proceedings of the 4th Federal Interagency Hydrologic Modeling Conference and the 9th Federal Interagency Sedimentation Conference,

Las Vegas, NV, 27 June–1 July, 2010. Session: sediment transport. CD-ROM ISBN 978-0-9779007-3-2.

Cavalli, M., Tarolli, P., Marchi, L., and Dalla Fontana, G.: The effectiveness of airborne LiDAR data in the recognition of channel-bed morphology, Catena, 73, 249–260, 2008.

Carling PA, Reader NA. 1982. Structure, composition and bulk properties of upland stream gravels. Earth Surface Processes and Landforms 7: 349-365.

Coveney, S., Stewart Fotheringham, A., 2011. Terrestrial laser scan error in the presence of dense ground vegetation. The Photogrammetric Record 26, 307-324.

Emmett WW. (1980): A Field Calibration of the Sediment-Trapping Characteristics of the Helley-Smith Bedload Sampler, US Geological Survey Professional Paper 1139, Washington, DC.

Erdogan, S., 2009. A comparision of interpolation methods for producing digital elevation models at the field scale. Earth Surf. Process. Landforms 34, 366-376.

Fonstad, M.A., Dietrich, J.T., Courville, B.C., Jensen, J.L., Carbonneau, P.E., 2013. Topographic structure from motion: a new development in photogrammetric measurement. Earth Surf. Process. Landforms 38, 421-430.

Gaudet J.M. (1994): Effect of Orientation and Size of Helley-Smith Sampler on Its Efficiency. Journal of Hydraulic Engineering, Vol. 120, No. 6, pp. 758-766

Haas, F., Heckmann, T., Hilger, L., and Becht, M., 2012: Quantification and Modelling of Debris Flows in the Proglacial Area of the Gepatschferner / Austria using Ground-based LIDAR, IAHS Publication, 356, 293–302

Hassan MA, Ergenzinger P. 2003. Use of tracers in fluvial geomorphology. In Tools in Fluvial Geomorphology, Kondolf GM, Piégay H (eds). John Wiley and Sons: Chichester; 397-423.

Habersack H.M. (2001): Radio-tracking gravel particles in a large braided river in New Zealand: a field test of the stochastic theory of bed load transport proposed by Einstein. Hydrological Processes, 15, 3, 377-391

Habersack H., Nachtnebel H.P., Laronne J.B. (2001): The continuous measurement of bedload discharge in a large alpine gravel bed river. Journal of Hydraulic Research, Volume 39, p. 125-133

Habersack H., Laronne J.B. (2001): Bedload texture in an alpine gravel bed river. Water Resources Research, Vol.37, No. 12, pp. 3359-3370

Habersack H., Seitz H., Laronne J.B. (2008): Spatio-temporal variability of bedload transport rate: analysis and 2D modelling approach, Geodinamica Acta, Vol.21/1-2, pp. 67-79

Habersack H., Seitz H., Liedermann M. (2010): Integrated Automatic Bedload Transport Monitoring. Published online as part of U.S. Geological Survey Scientific Investigations Report 2010-5091. p. 218-235. Retrieved June 15, 2013 from http://pubs.usgs.gov/sir/2010/5091/papers/Habersack.pdf

Habersack H., Kreisler A., Aigner J., Liedermann M., Seitz H., (2012): Spatio-temporal variability of bedload. In: Murillo Munoz, R.E. (Ed.), River Flow 2012 Vol. 1, 423-430; Taylor & Francis, London; ISBN 978-0-415-62129-8

Habersack H., Kreisler A., Aigner J., Seitz H., Laronne J., (in prep.): Integrated Bedload Transport Monitoring at the Drau-Isel system

Haschenburger J, Church M. 1998. Bed material transport estimated from the virtual velocity of sediment. Earth Surface Processes and Landforms 23: 791-808.

Hegg C., McArdell B.W., Badoux A. 2006. One hundred years of mountain hydrology in Switzerland by the WSL. Hydrological Processes 20: 371–376.

Helley E.J., Smith W. (1971): Development and calibration of a pressure-difference bedload sampler, open file report, Water Resour. Div., U. S. Geol. Surv. Menlo Park. Calif.

Heritage, G., Hetherington, D., 2005. The use of high-resolution field laser scanning for mapping surface topography in fluvial systems. IAHS Publication 291, 269-277.

Heritage, G., Hetherington, D., 2007. Towards a protocol for laser scanning in fluvial geomorphology. Earth Surf. Process. Landforms 32, 66-74.

Heritage, G., Milan, D.J., Large, A.R., Fuller, I.C., 2009. Influence of survey strategy and interpolation model on DEM quality. Geomorphology 112, 334-344.

Hodge, R., Brasington, J., Richards, K., 2009. IIn situ/I characterization of grain-scale fluvial morphology using Terrestrial Laser Scanning. Earth Surf. Process. Landforms 34, 954-968.

Hodgson, M., Bresnahan, P., 2004. Accuracy of Airborne Lidar-Derived Elevation: Empirical Assessment and Error Budget. Photogrammetric Engineering and Remote Sensing (Photogram Eng Rem Sensing) 70, 331-339.

Hohenthal, J., Alho, P., Hyyppa, J., Hyyppa, H., 2011. Laser scanning applications in fluvial studies. Progress in Physical Geography 35, 782-809.

Hugenholtz, C.H., Whitehead, K., Brown, O.W., Barchyn, T.E., Moorman, B.J., LeClair, A., Riddell, K., Hamilton, T., 2013. Geomorphological mapping with a small unmanned aircraft system (sUAS): Feature detection and accuracy assessment of a photogrammetrically-derived digital terrain model. Geomorphology.

James, L.A., Hodgson, M., Ghoshal, S., Latiolais, M., 2012. Geomorphic change detection using historic maps and DEM differencing: The temporal dimension of geospatial analysis. Geomorphology 137, 181-198.

Lamarre H, Mac Vicar B, Roy AG. 2005. Using passive integrated transponder (PIT) tags to investigate sediment transport in gravel-bed rivers. Journal of Sedimentary Research 75: 736-741. DOI: 10.2110/jsr.2005.059.

Lane, S.N., Westaway, R.M., Murray Hicks, D., 2003. Estimation of erosion and deposition volumes in a large, gravel-bed, braided river using synoptic remote sensing. Earth Surf. Process. Landforms 28, 249-271.

Laronne JB, Outhet DN, Duckham JL, Mc Cabe TJ. 1992. Determining event bedload volumes for evaluation of potential degradation sites due to gravel extraction, N.S.W., Australia. Erosion and Sediment Transport Monitoring Programmes in River Basins, Proceedings of the Oslo Symposium, August 1992, IAHS publ 210: 87-94.

Laronne JB, Outhet DN, Carling PA, Mc Cabe TJ. 1994. Scour chain employment in gravel bed rivers. CATENA 22: 299-306.

Lenzi M.A., Marchi L. 2000. Suspended sediment load during floods in a small stream of the Dolomites (northeastern Italy): Catena, v.39, pp. 267-282.

Liébault F, Laronne JB. 2008. Evaluation of bedload yield in gravel-bed rivers using scour chains and painted tracers: the case of the Esconavette Torrent (Southern French Prealps). Geodinamica Acta 21(1-2): 23-34. DOI: 10.3166/ga.21.23-34.

Liébault F, Bellot H, Chapuis M, Klotz S, Deschâtres M. 2012. Bedload tracing in a high-sediment-load mountain stream. Earth Surface Processes and Landforms 37(4): 385-399. 10.1002/esp.2245.

Liedermann M., Tritthart M., Habersack H. (2013): Particle path characteristics at the large gravel-bed river Danube: results from a

tracer study and numerical modelling. Earth Surface Processes and Landforms 38(5): 512-522.

Lindsay, J.B., Ashmore, P.E., 2002. The effects of survey frequency on estimates of scour and fill in a braided river model. Earth Surf. Process. Landforms 27, 27-43.

Mao L., Cavalli M., Comiti F., Marchi L., Lenzi M.A., Arattano M. 2009. Sediment transfer processes in two Alpine catchments of contrasting morphological settings. J. Hydrol. 364:88-98.

Mao L., Comiti F., Lenzi M.A. 2010. Bedload dynamics in steep mountain rivers: insights from the Rio Cordon experimental station (Italian Alps). In Bedload-surrogate Monitoring Technologies, Gray JR, Laronne JB, Marr JDG (eds), US Geological Survey Scientific Investigations Report 2010–5091. US Geological Survey: Reston, VA; 253 265.

Maraga F., Arattano M., Pelissero C. 2011. Coarse sediment dynamics in field instrumented streams. In Epitome 2011, Volume 4, pag. 68. Proceedings of Geoitalia 2011 - VIII Forum Italiano di Scienza della Terra.

Meng, X., Currit, N., Zhao, K., 2010. Ground Filtering Algorithms for Airborne LiDAR Data: A Review of Critical Issues. Remote Sensing 2, 833-860.

Milan, D.J., Heritage, G., Hetherington, D., 2007. Application of a 3D laser scanner in the assessment of erosion and deposition volumes and channel change in a proglacial river. Earth Surf. Process. Landforms 32, 1657-1674.

Mirijovsky, J., 2012. UAV Photogrammetry in Fluvial Geomorphology. In: SGEM2012 12th International Multidisciplinary Scientific GeoConference and EXPO. Stef92 Technology.

Mizuyama T, Fujita M, Nonaka M. (2003): Measurement of bed load with the use of hydrophones in mountain torrents. In Erosion and Sediment Transport Measurement in Rivers: Technological and Methodological Advances, Bogen J, Fergus T, Walling DE (eds). IAHS Publication 283, International Association of Hydrological Sciences: Wallingford; pp. 222–227.

Mizuyama, T., Oda, A., Laronne, J.B., Nonaka, M., Matsuoka, M. (2010 a) Laboratory Tests of a Japanese Pipe Geophone for Continuous Acoustic Monitoring of Coarse Bedload. Published online as part of U.S. Geological Survey Scientific Investigations Report 2010-5091, pp 319-335.

Mizuyama, T., Laronne, J.B., Nonaka, M., Sawada, T., Satofuka, Y., Matsuoka, M., Yamashita, S., Sako, Y., Tamaki, S., Watari, M., Yamaguchi, S. & Tsuruta, K. (2010 b): Calibration of a passive acoustic bedload monitoring system in Japanese mountain rivers. Published online as part of U.S. Geological Survey Scientific Investigations Report 2010-5091, pp 296-318.

Mühlhofer L. (1933): Schwebstoff- und Geschiebemessungen am Inn bei Kirchbichl (Tirol). Wasserkraft und Wasserwirtschaft 28Jg., S. 37-41.

Morche, D., Witzsche, M., Schmidt, K.-H., 2008. Hydrogeomorphological characteristics and fluvial sediment transport of a high mountain river (Reintal Valley, Bavarian Alps, Germany). Zeit fur Geo Supp 52, 51-77.

Reid I., Layman J.T. & Frostick L.E. (1980): The continuous measurement of bedload discharge. Journal of Hydraulic Research 18, 243-249.

Rickenmann D., Fritschi B. 2010. Bedload transport measurements using piezoelectric impact sensors and geophones. In Bedload-surrogateMonitoring Technologies, Gray JR, Laronne JB, Marr JDG (eds), US Geological Survey Scientific Investigations Report 2010–5091. US Geological Survey: Reston, VA; 407–423. http://pubs.usgs.gov/sir/

Rickenmann D., Turowski J.M., Fritschi B., Klaiber A., Ludwig, A. 2012. Bedload transport measurements at the Erlenbach stream with geophones and automated basket samplers. Earth Surf. Process. Landf. 37: 1000-1011.

Rickenmann D., Turowski J., Fritschi B., Wyss C., Laronne J., Barzilai R., Reid I., Kreisler A., Aigner J., Seitz H., Habersack H. (in prep.): Bedload transport measurements with impact plate geophones: comparison of sensor calibration at different gravel-bed streams. Earth Surface Processes and Landforms

Scheidl, C., Rickenmann, D., Chiari, M., 2008. The use of airborne LiDAR data for the analysis of debris flow events in Switzerland. Nat. Hazards Earth Syst. Sci 8, 1113-1127.

Schürch, P., Densmore, A.L., Rosser, N.J., Lim, M., McArdell, B.W., 2011. Detection of surface change in complex topography using terrestrial laser scanning: application to the Illgraben debris-flow channel. Earth Surf. Process. Landforms 36, 1847-1859.

Sear DA, Lee MWE, Oakey RJ, Carling PA, Collins MB. 2000. Coarse sediment tracing technology in littoral and fluvial environments. In Tracers in Geomorphology, Foster IDL (ed). John Wiley and Sons: Chichester; 21-55.

Sharma, M., Paige, G.B., Miller, S.N., 2010. DEM Development from Ground-Based LiDAR Data: A Method to Remove Non-Surface Objects. Remote Sensing 2, 2629-2642.

Vericat D., Chruch M., Batalla R.J. (2006): Bed load bias: Comparison of measurements obtained using two (76 and 152 mm) Helley-Smith samplers in a gravel bed river. Water Resources Research, Vol.37, No. 12, pp. 3359-3370

Vericat, D., Brasington, J., Wheaton, J., Cowie, M., 2009. Accuracy assessment of aerial photographs acquired using lighter-than-air blimps: low-cost tools for mapping river corridors. River Res. Applic. 25, 985-1000.

Villi V., Gatto G., Caleffa G. (1985): Measures of solid transport in the small dolomitic basin "Rio Missiaga" (Belluno - Italy). C.N.R.-PAN meeting, Torino, 5-7 Dic. 1984, pp. 333-350

Westoby, M. J., Brasington, J., Glasser, N. F., Hambrey, M. J., and Reynolds, J. M.: 'Structure-from-Motion' photogrammetry: A low-cost, effective tool for geoscience applications, Geomorphology, 179, 300–314, doi:10.1016/j.geomorph.2012.08.021, 2012.

Wheaton, J.M., Brasington, J., Darby, S.E., Sear, D.A., 2010. Accounting for uncertainty in DEMs from repeat topographic surveys: improved sediment budgets. Earth Surf. Process. Landforms 35, 136-156.

Williams, R., Brasington, J., Vericat, D., Hicks, M., Labrosse, F., Neal, M., 2012. Monitoring Braided River Change Using Terrestrial Laser Scanning and Optical Bathymetric Mapping. In: Smith, M., Paron, P., Griffiths, J.S. (Eds.), Geomorphological mapping. Methods and applications. Elsevier, Amsterdam [etc.], pp. 507-532.

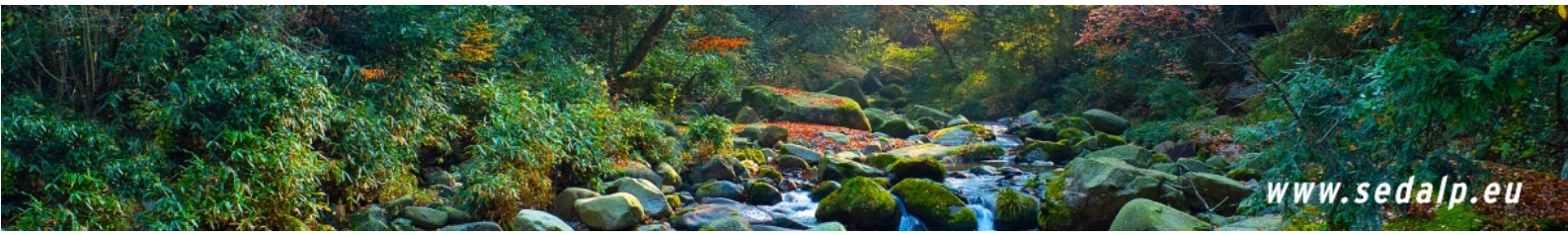

Part II

Protocol for Debris-flow Monitoring

WP5 - Action 5.2

Protocols on standardized data collection methods in sediment transport monitoring for transboundary exchange

Lead authors: Marco Cavalli, Lorenzo Marchi, Massimo Arattano (PP4)

Contributors: Francesco Comiti (PP1), Luca Schenato (PP4), Frédéric Liébault (PP7)

June 2013

Contents

1 Introduction

Monitoring of debris flows in instrumented catchments permits collection of data on these phenomena and provides a valuable link with geomorphological and topographical observations of erosion, sediment supply and channel evolution. The recorded data can serve as a basis for implementing of early warning systems that provide defense against debris-flow risk. The quantification of sediment volumes transported by debris flows along with their temporal frequency, timing, flow characteristics (i.e. velocity, flow depth, peak discharge, density) are of crucial importance for hazard assessment, land-use planning and design of torrent control structures. In addition, instrumented basins provide high-quality information for deriving regional thresholds of rainfall intensity and/or cumulated values for debris-flow triggering to be used in warning systems.

Japan and China have pioneered debris-flow monitoring (Okuda et al., 1980; Zhang, 1993) and sites instrumented in these countries still play a significant role in debris-flow research, also thanks to the long time series of recorded data (Hu et al., 2011a, b; Suwa et al., 2011). In Taiwan, the frequent occurrence of high-magnitude debris flows with severe damage to settlements has urged the installation of equipment for monitoring debris flows and for issuing warnings in a number of sites (Yin et al., 2011). Amongst early experiences on instrumental observations of debris flows in the United States, are the monitoring campaigns by Pierson (1986) in channels on the flanks of Mount St. Helens. More recently, the installation of monitoring equipment at Chalk Cliffs, a small, very active catchment in the Colorado Rocky Mountains, has started providing valuable information and data on debris-flow triggering and flow dynamics (Coe et al., 2008; McCoy et al., 2011). In Europe, the first catchment instrumented for debris-flow monitoring was probably the Moscardo Torrent in the Eastern Italian Alps (Arattano et al., 1997; Marchi et al., 2002). Other sites were

instrumented in the late 1990s and early 2000s in Italy (Tecca et al., 2003) and Switzerland (Hürlimann et al., 2003). Amongst these monitoring sites, the Illgraben catchment (Switzerland) deserves to be mentioned because of innovative measurements on forces and pore fluid pressure in debris flows (Mc Ardell et al., 2007) and channel-bed erosion (Berger et al., 2011). Recent development of monitoring activities in Europe, which include installations in Austria (Kogelnig et al., 2011), France (Navratil et al., 2012; 2013b), and Spain (Hürlimann et al., 2011) indicates the high interest for this sector of debris-flow studies.

The number of monitoring sites and the amount of recorded data on debris flows remains still limited if compared to landslides and fluvial sediment transport. Moreover, the large variability of debris-flow features, their dependence on local topographical, geological and climate conditions makes the collection of more data in instrumented catchments of the utmost importance.

This protocol aims at describing minimum requirements for a debris-flow monitoring site and illustrating the existing sensors and methods of measurements and data collection. In the SedAlp Project several catchments are instrumented for debris-flows monitoring: Rio Gadria by the Autonomous Province of Bozen-Bolzano (PP1) with the collaboration of CNR-IRPI (PP4), Rio Chiesa by ARPAV (PP2), Moscardo Torrent by CNR-IRPI (PP4), Manival and Réal torrents by Irstea (PP7). Monitoring concepts of these pilot areas were used to draft the protocol; devices and measurements methods implemented in European debris-flow monitoring sites outside the project were also considered in order to provide a comprehensive view of existing methods for debris-flow monitoring.

1.1 Debris-flow warning system

It is nowadays recognized that a combination of structural and non-structural measures is needed to cope with debris-flow risks. Non-structural

measures for debris-flows control aim mainly to diminish the vulnerability of a certain area, by reducing either permanently (e.g. land-use planning) or temporarily (warning systems) the probability that humans and their goods might be hit by a debris flow.

Warning systems for debris flows can be classified into two main types: advance warning and event warning (Hungr et al. 1987; Arattano and Marchi, 2008). Advance warning systems predict the possible occurrence of a debris-flow event beforehand, by monitoring the possible onset of triggering conditions. These warnings are usually obtained by comparing precipitation forecasts with local precipitation thresholds for triggering (e.g. Caine, 1980; Wilson et al., 1993; Bacchini and Zannoni, 2003; Guzzetti et al., 2008). On one hand, these approaches may permit lead times of some hours. However, on the other hand, the warnings are heavily affected by the uncertainties in the precipitation forecasts and in the estimates of local threshold curves. These approaches are very useful for warnings at regional scale, where lower spatial resolution is required. An event warning is issued after the actual detection of debris flows, based on measures from various types of sensors, such as wire sensors, ground vibration sensors or stage meters (Arattano and Marchi, 2008), upstream of a vulnerable site (e.g. road, town). Owing to such characteristics, event warning is potentially very reliable (Chang, 2003; Badoux et al., 2009), even though the time interval between the detection and the arrival of the debris flow to the vulnerable site is very short and the need of maintenance of the warning system increases the costs. These limitations are intrinsic to debris-flow warning systems and cannot be easily eliminated, but refinements in debris-flow detection and alarm dissemination technologies may contribute to improve the warning effectiveness.

2 Debris-flow monitoring devices and methods

A number of devices and methods have been developed for monitoring debris flows. Reviews of devices and methods which may be used to obtain the warning and modeling information for debris flow have been provided by Itakura et al. (2005) and Arattano and Marchi (2008). This protocol focuses on the sensors and methods commonly employed to measure the most relevant parameters for debris-flow investigation. Table 1 summarizes the main parameters that should be measured in a debris-flow monitoring site and the sensors that can be employed to achieve the measurements. Table 2 lists a number of additional parameters that can be also measured to collect more information on debris flows.

The mere occurrence of a debris flow, which provides limited information on the characteristics of the event, but could prove sufficient for warning purposes, may be detected by means of different sensors (wire sensors, photocells, ultrasonic/laser/radar sensors, geophones). Detection of debris flows is possible also by using pendulums hung over the channel: from the tilting of the pendulum or the impact of the flowing mass on it (Figure 1).

Figure 1 A pendulum installed in a channel to detect debris-flow occurrence (Rotolon catchment, Italy).

Table 1 Main debris-flow parameters and measuring devices

Rainfall amount and intensity
Raingauge
Flow characteristics (visual recognition)
Camera, Videocamera
Peak flow depth
Theodolite or GPS (post-event survey), wire sensors, photocells, ultrasonic sensors, radar sensors, laser sensors
Debris-flow hydrograph
Ultrasonic sensors, radar sensors, laser sensors
Ground vibration
Seismometer or geophones (velocimeters, accelerometers)
Mean flow velocity, peak discharge and volume (derived variables)
Ultrasonic sensors, radar sensors, laser sensors

Table 2 Additional debris-flow parameters and measuring devices

Infrasound Microphones
Surface velocity Electromagnetic doppler speedometers, Large Scale Particle Image Velocimetry (LSPIV) applied to video recordings, speed sensors based on spatial filtering velocimetry
Basal forces (normal and shear stress) Load cells
Fluid pore pressure Pressure sensors
Impact force Pressure mark gauges, strain gauges
Erosion depth and timing
Resistors in erosion sensor column
Topography of debris flow deposits Terrestrial Laser Scanner, Theodolite, GPS
Channel storage and sediment sources changes Airborne LiDAR, Terrestrial Laser Scanner, Theodolite, GPS

2.1 Rainfall

Rainfall measurement provides essential information for deriving regional thresholds of rainfall intensity and/or cumulated values for debris-flow triggering. Tipping bucket rain gauges (Figure 2) are commonly used for measuring rainfall in debris-flow monitoring sites. As most debris flows are triggered by intense rainfall, a high data acquisition rate has to be set up (1-5 min) and a high rainfall resolution (i.e. amount of water required to make the bucket tip producing an electrical signal) is also suggested (0.2 mm). Recording the time of occurrence of bucket tipping is an alternative method of rainfall data acquisition. Rain gauges must be positioned on a flat surface, located in open sites avoiding sheltering by trees or buildings, and installed at height >1.5 m above ground. An easily accessible site facilitates regular visits of the instrument for maintenance and data retrieving, in the case data are stored in dataloggers. However, data can also be transmitted by radio, GSM, UMTS if the monitoring site is served by at least one of these technologies. A wise positioning of rain gauges should include at least one instrument close to the expected debris-flow triggering area.

Figure 2 A rainfall gauge installed upslope of a debris-flow initiation area

2.2 Flow characteristics

Images and video recordings give an invaluable contribution to the recognition and interpretation of flow processes and effectively support quantitative monitoring performed by other sensors designed to record debris-flow depth and hydrographs. Amongst relevant debris-flow features that can be documented by video camera recordings, we mention the following:

- variations in solid concentration and particle size, both between different debris flows and within the same event;
- onset of turbulence corresponding to decrease in solid concentration (typically in the final phase of a debris-flow surge);

- presence and characteristics of precursory surges in the initial phase of a debris flow and secondary surges in the recession limb;
- transport of large wood by the debris flow.

In addition to the visual interpretation, video recordings provide the basis for automated or semi-automated recognition of important features of debris flows, such as grain size distribution (Genevois et al., 2001) or the presence of large boulders (Gomez and Lavigne, 2010). Moreover, several studies have demonstrated the suitability of video recordings (e.g. Arattano and Marchi, 2000; Genevois et al., 2001; Zhang and Chen, 2003) for recognizing debris-flow features in different parts of a channel reach. Surface velocity assessment from oblique video recordings could also be possible applying Large Scale Particle Image Velocimetry (LSPIV) algorithms. These methods are successfully used to measure velocities at the free surface of water streams (Muste et al., 2008). Zenithal recordings, achieved by video cameras installed vertically above the channel, shot a much smaller area, but permit easier assessment of flow characteristics, such as surface velocity distribution along the cross-section and particle size distribution of transported clasts. Cameras provided with image processing software are able to automatically evaluate the debris flow material movement (moving detection). This kind of software is able to recognize all the objects in function of their electromagnetic spectrum and to filter the data, in order to erase the noise elements such as the rainfall, allowing identifying only the moving debris flow material and thus potentially to issue a warning signal.

To overcome the limitation of night view, videocameras can be installed with spotlights (Figure 3), which activation can be triggered by the exceeding of a certain threshold of data recorded by other sensors (e.g. raingauges, stage sensors). Alternatively, thermal cameras able to register the electromagnetic wave released by each material in function of its own

temperature could be used to record images at night, but the resolution of these devices is usually lower than that of normal videocameras.

Figure 3 A videocamera with spotlight (Gadria catchment, Italy)

2.3 Peak flow depth

Without fixed instrumentations, the maximum debris flow depth can be measured during post-event surveys using theodolites or differential GPS thanks to the marks left on channel banks (Figure 4). Particular care must be taken to differentiate between the tracks left by the debris flow surface and the tracks left by the debris flow splashes (Aulitzky, 1989).

A set of wires stretched at different levels across a cross-section can be also employed to monitor maximum depth of debris flows. These wires can detect the maximum depth according to the level of the highest wire that has been broken by the flow and also make it possible to record the time of occurrence of the surge at the instrumented site. However, after they have been broken, these devices cannot provide information about the height of further surges that follow the main one or about subsequent debris flows; they need to be reset each time after a debris flow. Photocells and infrared photobeam sensors can be utilized as a tool to detect debris flows (Chang,

2003). The flowing mass interrupts the beams emitted by the sensors, making it possible to detect the passage of the wave. If several sensors are installed at different heights at the same cross-section, it is also possible to approximately measure the peak flow stage.

Figure 4 An example of mud mark on a bank after the passage of a debris flow on the Réal Torrent in the French Alps; this kind of marks can be used to measure the flow depth during the peakflow discharge

2.4 Debris-flow hydrograph

Debris flow depth represents the basis for the computation of other relevant variables such as flow velocity, discharge and volume. Different types of stage sensors can be used to monitor and record flow depth.

Ultrasonic sensors hung over the channel are the most used sensors to record debris-flow depths and hydrographs (Figure 5). These sensors are typically used to measure the hydrometric level in rivers and lakes. The strong and rapid variability of flow height with time in debris flows requires much shorter logging intervals between two consecutive recordings (1-2 seconds) than that used in water level measurements. Radar and laser sensors have also been used, similarly to ultrasonic sensors, to measure flow depth and record stage hydrographs of debris flows (Hürlimann et al, 2003; McArdell et al., 2007). Ultrasonic, radar and laser sensors work on a similar principle: the antenna of the sensor emits pulses that are reflected by the surface of the debris flow and received by the antenna as echoes. The running time of the pulses from emission to reception is proportional to the distance and hence to the level. The determined level is converted into an appropriate output signal and outputted as measured value. Badoux et al. (2009) outline about advantages and drawbacks of these three types of sensors: “Ultrasonic sensors are troublesome because under conditions of rapidly changing flow depth and splashing on the surface of the flow they sometimes do not return a signal (Hürlimann et al. 2003). Laser sensors provide high-quality data for debris flows (e.g., McArdell et al. 2007), but do not provide a useable signal for flood or hyper-concentrated flows. Radar sensors have a built in smoothing algorithm that provides a stable signal under conditions of rapidly changing flow depth or splashing on the surface of the flow, but the signal is delayed by a few seconds and changes in surface elevation are smoothed in comparison with laser sensors, making them somewhat less useful for research but reliable for warning”.

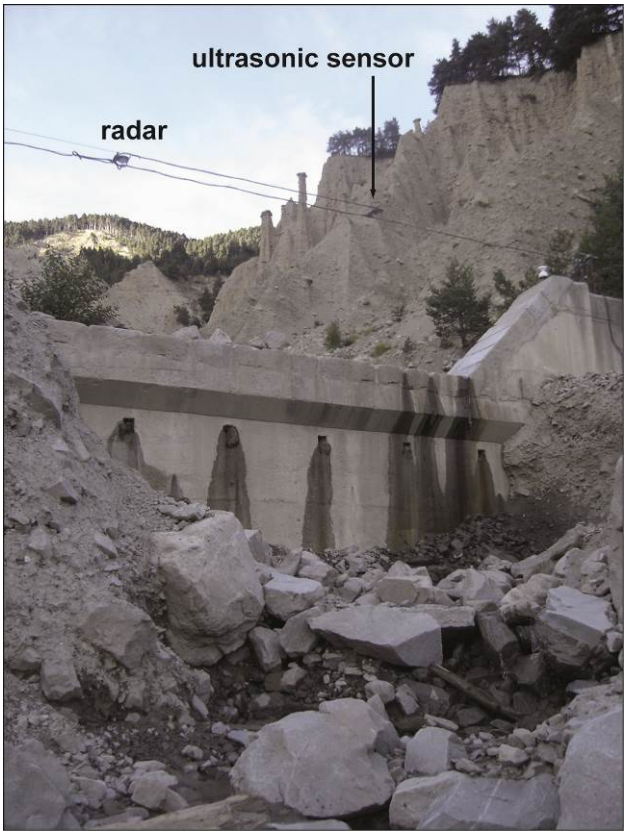

Figure 5 Example of ultrasonic and radar sensors deployed on a cable above a check-dam on the Réal Torrent in the French Alps

2.5 Ground vibration

The passage of a debris-flow wave induces strong ground vibrations and underground sounds which can be recorded by different types of sensors (accelerometers, velocimeters, microphones; Zhang, 1993; Arattano, 1999; Suwa et al., 2011). The output signal of seismic sensors is a voltage proportional to the ground oscillation velocity that may be processed in different ways to extract more useful information, such as debris-flow hydrographs. An important advantage of ground vibration sensors is that they can be installed at a safe distance from the channel bed, overcoming an important limitation of other types of sensors which need to be hung over the channel and thus are more prone to damage. The vibration frequency associated with debris flows generally span the range from few Hz up to 300 Hz (Huang et al., 2007). It has to be noted that according to

the signal processing theory, the sampling rate at which the signal from the geophone has to be sampled to avoid aliasing must be at least twice the highest frequency of the signal itself. Furthermore, it is worthy to mention that attenuation of ground vibration in soil is extremely high; this issue requires multiple geophones to be deployed and/or an opportune positioning. The attenuation, furthermore, is related to soil density, water content, matrix potential and porosity and generally scales inversely with respect to the frequency. Subsequently, the spectrum is usually dominated by lower frequency components. Nonetheless, due to the underlined requirements about sensitivity and sampling frequency, the electronics required to correctly sample the signal from the geophones and preserve data integrity present a significant challenge.

The output signal of seismic sensors is currently processed with three different methods: the amplitude (Arattano, 1999), the impulses (Abancó et al., 2012), and the integration (Navratil et al., 2013a) methods.

Seismic data processing with the amplitude method consist in transforming the signal from analogical to digital and then to calculate the mean absolute value every second (amplitude) to reduce the data amount. The amplitude (A) can be calculated as:

$$A = \frac{\sum_{i=1}^{n} |v_i|}{n} \quad (1)$$

where v_i is the ground oscillation velocity, and n is the number of digital samples in each interval of recording.

The data processing of debris-flow recordings obtained through ground vibration sensors returns graphs that strictly resemble the hydrographs recorded through ultrasonic, radar or laser sensors. A comparison between an hydrograph (black line) and an amplitude-versus-time-graph obtained with the previously described procedure (red line) for an event occurred in the Moscardo Torrent on June 22, 1996 is shown in Figure 6.

The impulses method is adopted in Switzerland and Spain (Abancó et al., 2012) monitoring sites to reduce the data amount and it consists in transforming the continuous signal (thick line in Figure 7) into a pulse signal (thin line in Figure 7) and then counting the number of impulses per each time interval. The impulses method requires the identification of a threshold value (red line in Figure 7) above which starting to count the impulses. If the chosen threshold is too low then the distinction between the phases of the event might become impossible. Another limitation of this method is the loss of information regarding the intensity of the signal. While the digitalization used by the amplitude method still conserves information regarding the intensity, namely its mean value, the transformation into impulses loses this residual information.

The integration method is implemented in France (Réal and Manival monitoring stations). An electronic signal processing unit is used to transform the output voltage of the geophone into an integrated signal that is sampled by the data logger unit (Campbell CR1000) at a frequency of 5 Hz. The signal processing unit is an electronic printed circuit specifically designed for the conditioning of analog signal from geophones. The unit first transforms the output voltage of the geophone into a rectified unidirectional signal (negative voltages are transformed into positive voltages). The rectified signal is then filtered with a 2.5 Hz cutoff frequency low-pass filter. The cutoff frequency was set at half the sampling frequency of the data logger to respect the Shannon criteria. This filtering is equivalent to applying a moving average on the raw signal, with a time period equal to 400 ms (Figure 8). The filtered signal is amplified and transformed into tension (mA) to be transported on long distances (up to 300 m). The main advantage of this method is that the geophone data can be sampled at a low frequency (5 Hz) while conserving the integral of the raw signal (total energy) from the geophone. It is nevertheless clear that

the frequency spectrum of the ground vibrations is lost, as well as the maximum range of ground vibration amplitudes.

Soil properties of the river banks and location of each geophone determine specific offset and gain. Preliminary tests have been carried out with heavy boulders (approx. 10 kg) that were manually thrown into the torrent channel (3–4 m high) near geophones (Navratil et al., 2013a). Those tests showed that (1) the system can detect very low-magnitude ground vibrations, and (2) such recordings are consistent with nature and distance of triggering source from the geophone. By the same tests, it is also possible to calibrate the geophones. The magnitude of the signal mainly depends on the location of the geophone (on a bank, a boulder on a bank, and a check-dam, respectively), and, marginally, on the composition of the soil from the source to the geophone. Ultimately, it was found that the geophone fixed on big boulders embedded in a gravel deposit responds better. Remarkably, that data acquisition method has been successfully tested during several debris flows which occurred on the Réal Torrent since 2011 (Figure 9).

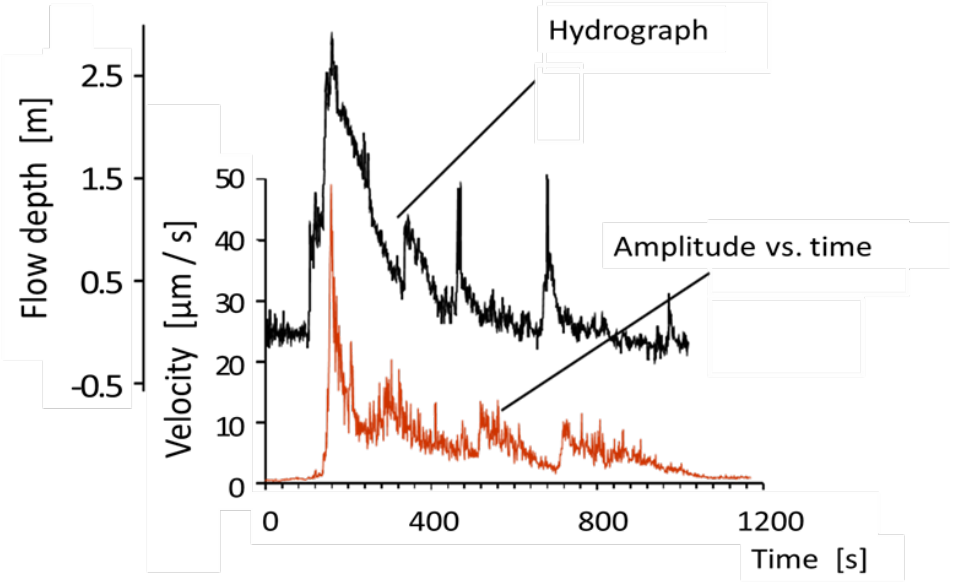

Figure 6 Comparison between an hydrograph (black line) and an amplitude-versus-time-graph (red line) for an event occurred in the Moscardo Torrent on June 22, 1996. The small differences between the hydrograph and the amplitude vs. time graph are due to the different locations of the sensors (geophones are installed around 1 km upstream ultrasonic sensors).

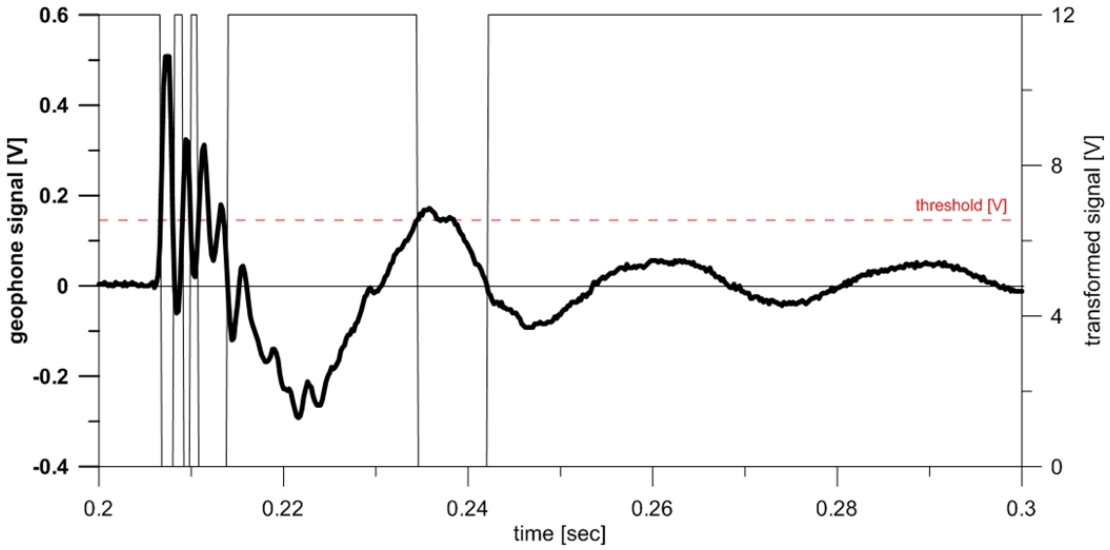

Figure 7 The transformation of the signal in the impulses method (from Abancó et al., 2012)

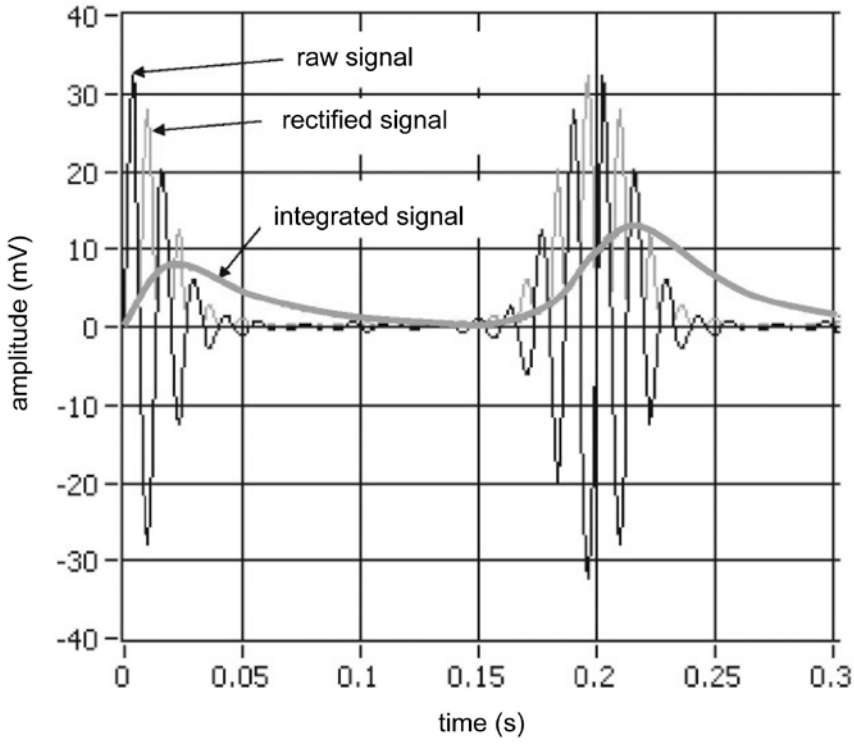

Figure 8 Numerical example of signal processing implemented in the integration method

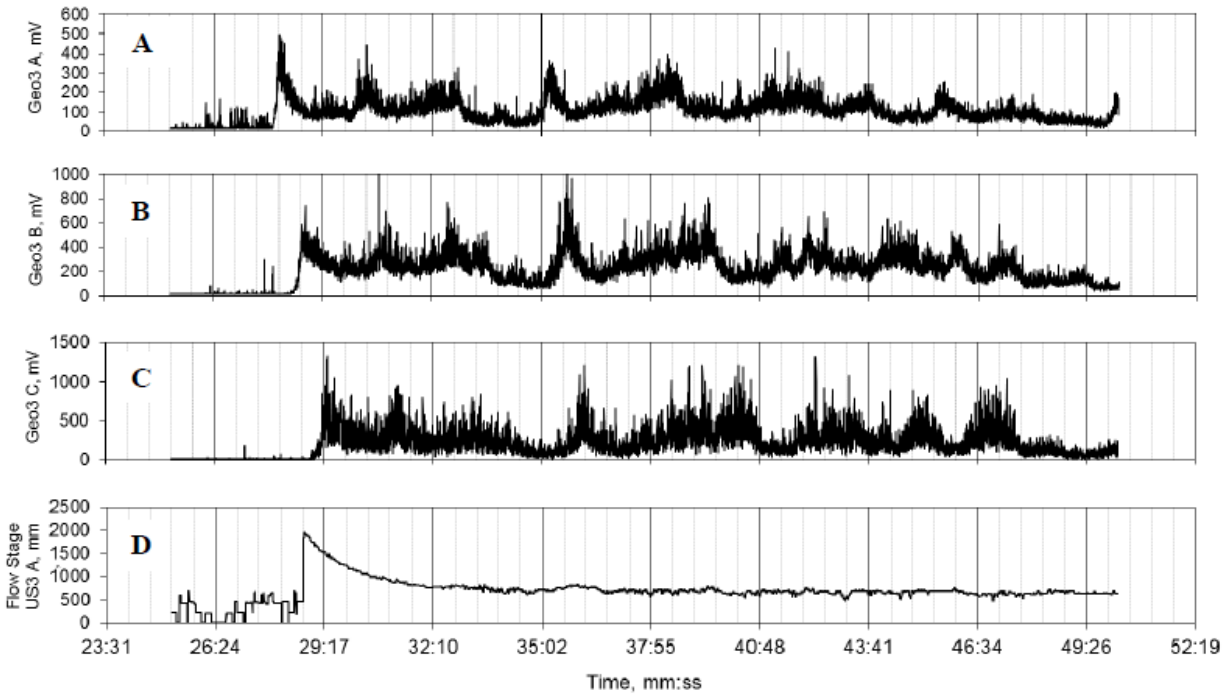

Figure 9 Geophone recordings at Réal Torrent during the 29 June 2011 debris flow. (A) Upstream geophone Geo3A. (B) Middle stream geophone (Geo3B). (C) Downstream geophone (Geo3C). (D) The flow stage recorded by the ultrasonic sensor (US3_A at the same location as Geo3B); the reference elevation for US measurements (0 cm) corresponds to the channel bottom (From Navratil et al., 2013b)

Fiber optic sensors have also been proposed for monitoring ground vibrations caused by debris flows. The major advantage over conventional electronic-based sensors is the ability to separate the sensors from the electronics without any significant degradation in performance. This puts away the electronics from the hostile sensing environment. Furthermore, the performance matches or exceeds the performance of standard geophones and the sensor is intrinsically safe and immune to EMI/RFI.

To our knowledge, there are very few examples in literature of employing fiber optic sensors for debris flow-induced ground vibration (Yin, 2012; Huang et al., 2012), but there are a large number of papers proposing

optical fiber geophones for similar application (e.g., oil & gas reservoir and micro-seismic exploration) so it is very likely this technology to break into this field and successfully compete with traditional geophones. Up to now, the large cost of deployment and maintaining represents the main drawback.

2.6 Mean flow velocity

The characteristic steep debris-flow front can be detected and recognized in the hydrographs allowing to easily perform mean front velocity measurements. By placing a pair of ultrasonic/radar/laser sensors or geophones at a known distance along a torrent, mean front velocity can be measured as the ratio between the distance between the sensors and the time interval elapsed between the arrival of the front at the two gauging sites (Figure 10). Mean velocity could also be computed from the records of other sensors using the same principle (e.g., wire detectors, photocells, microphones, etc.).

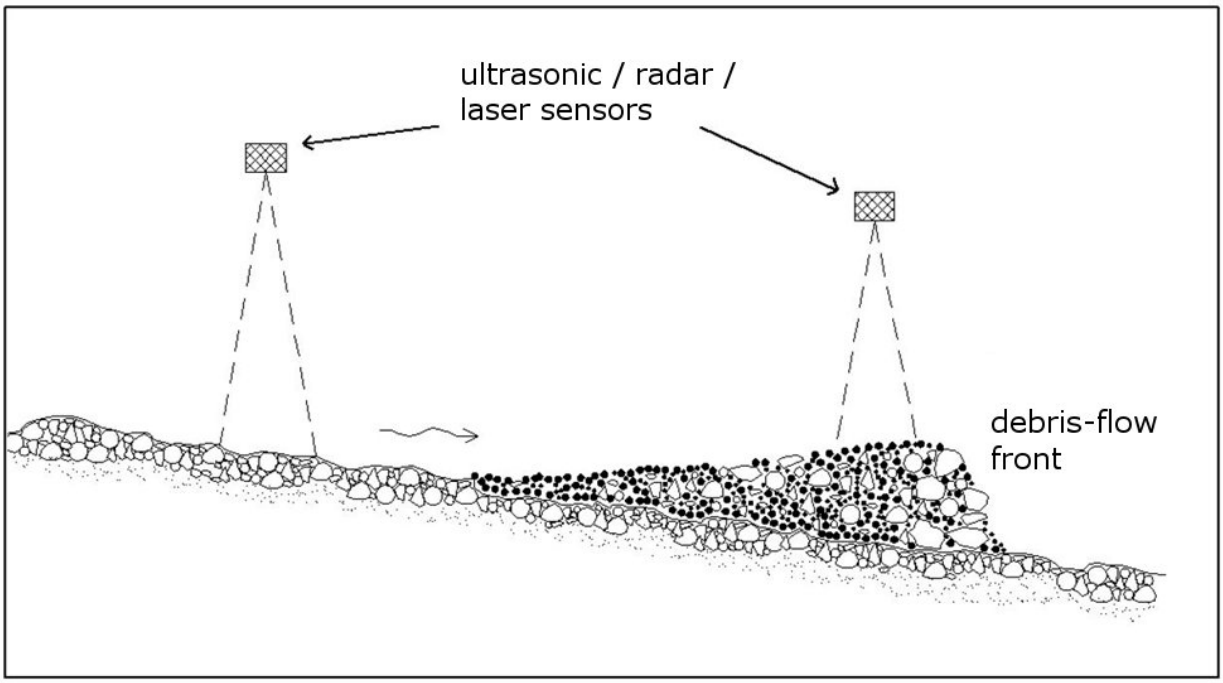

Figure 10 Flow depth measurement at two monitoring stations makes it possible to assess mean front velocity; (the horizontal scale is shortened with regard to both the distance between the sensors and the debris flow profile) (modified from Arattano and Marchi, 2008)

When ultrasonic/radar/laser sensors and seismic devices are used to measure mean front velocity, debris-flow front and/or other specific recognizable features must be present in their graphs. However such features may not be always present in the graph. The use of cross correlation techniques, that are commonly used in signal processing, may allow the use of graphs that do not show a clear front or other evident recurrent features, to estimate at least the mean velocity of the entire wave. In general, cross-correlation can be defined as the correlation of a series with another series, shifted by a particular number of observations and its function can be expressed as follow:

$$\phi_{xy}(\tau) = \sum_{t=-\infty}^{+\infty} x_t y_{t+\tau} \qquad (2)$$

where x_t is the function that expresses the recorded signal at the upstream sensor at the time t and $y_{t+\tau}$ is the function that gives the recorded signal at the downstream sensor at the time $t+\tau$. The maximum value of the function ϕ_{xy} allows an estimation of the value of τ., that is the time needed by the debris flow to propagate between the two sensors, and allows to determine the mean velocity of the wave (Figure 11). If the distance between the two locations is known, the velocity can then be easily assessed.

Therefore, given a certain phenomenon that produced a recorded at two different locations, the cross correlation analysis allows to determine, with an objective method, the time interval elapsed between the appearance of that phenomenon at the first and at the second location.

The cross correlation technique may allow a comparison between the mean front velocity, when a front is present, and the mean velocity of the entire wave, which may be significantly different sometimes. As far as the estimation of the volume of the debris flow using two hydrographs is concerned, the use of the velocity of the entire wave would be preferable to get a more consistent estimation when it differs from the mean front velocity.

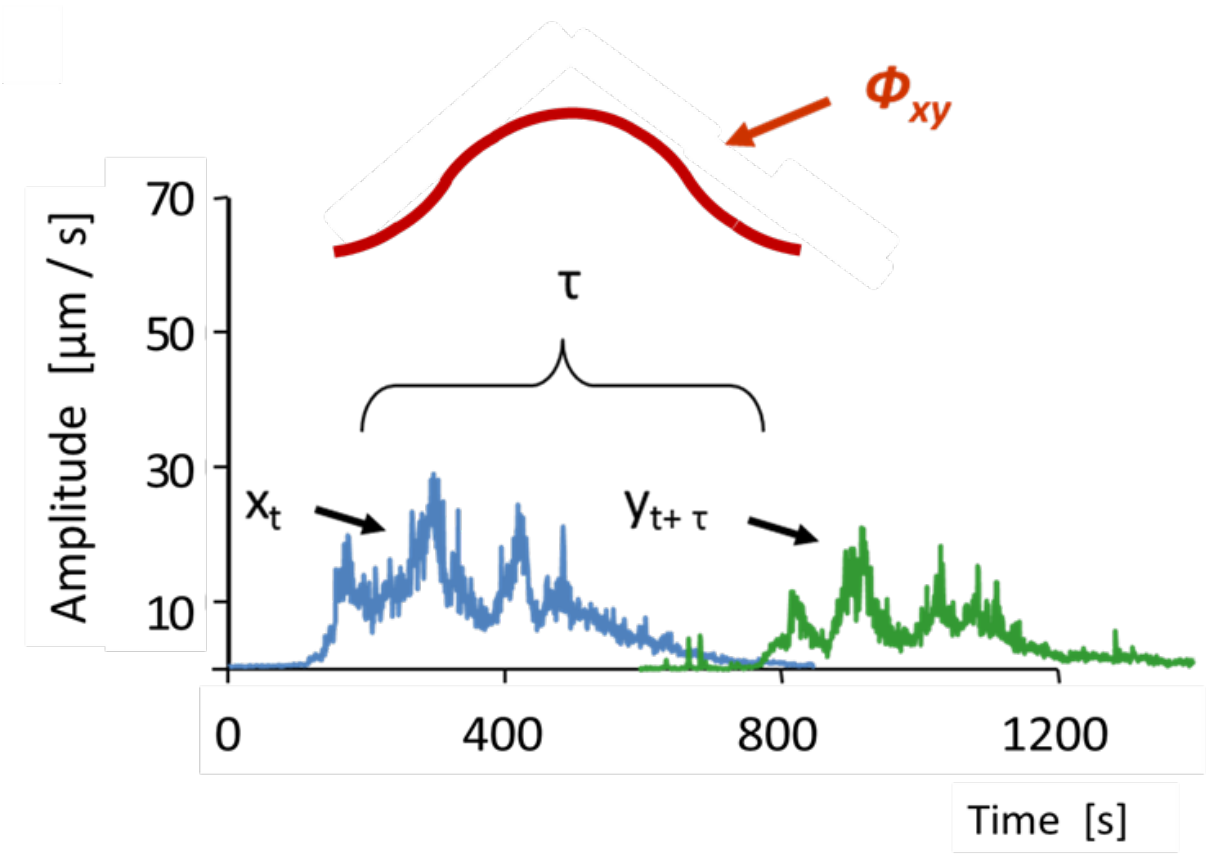

Figure 11 Cross correlation applied to debris-flow amplitude data from geophones records.

2.7 Peak discharge and volume

The measurement of debris-flow depth and the assessment of mean flow velocity provide the elements for estimating discharge and total debris flow volume. The flow area occupied at different times along a debris-flow wave is obtained from stage measurements and topographic surveys of the

cross-section geometry. Discharge can be computed as the product of the mean flow velocity by the cross-sectional flow area. Total discharged volume is then computed by integrating debris flow discharge on the hydrograph:

$$Vol = U\int_{t_0}^{t_f} A(t)dt \qquad (3)$$

where *A(t)* is the cross section area occupied by the flow at the time *t*, *U* is the mean flow velocity, t_0 is the time of arrival of the surge at the gauging site and t_f - t_0 is the overall time interval of the debris flow. This approach can be applied only in cross-sections in which the debris flow did not cause significant topographic changes. The approach to computing the flowing volume presented in eq. 3 assumes that the material flows through the considered section at a constant velocity during the surge. Usually the value of *U* is assumed as the value of the mean velocity of the front. However measurements, carried out using video pictures, have shown that an increase of velocity may occur behind the front and then surface velocity remains higher than front velocity for a significant portion of the debris-flow wave (Marchi et al., 2002). Using mean front velocity in eq. 3 could then result in an underestimation of debris-flow volumes.

Since mean velocity may vary remarkably during the surge, debris-flow volumes assessed using eq. 3 should be considered as approximate estimates. If flow velocity measurements are available for various phases of the event, they can be used to refine the volume assessment. Since mean front velocity and the mean velocity of the entire wave, obtained through cross-correlation, may significantly differ sometimes, as mentioned previously, the use of the latter would be preferable to get a more consistent estimation when this difference is significant.

2.8 Overview of additional devices

In addition to the devices and methods employed for monitoring debris-flow main parameters described in the previous sections, several additional parameters can be also measured to collect more information on debris flows (Table 2). Infrasound monitoring system can be used for debris-flow monitoring purposes (Zhang et al., 2004; Chou et al., 2007; Kogelnig et al., 2011). Infrasound signals generated by mass movement have a specific amplitude and occupy a relatively noise-free band in the low-frequency acoustic spectrum. The low-frequency fluctuations in the air can be detected by an infrasound microphone (Kogelnig et al., 2011). The main advantages of this method are similar to those of geophones (e.g., monitoring with a safe distance from the channel bed) whereas problems are mainly given by noise induced from other sources (e.g., human activity, wind). Doppler speedometers, which operating principle is based on measuring the frequency of radio waves reflected by a moving object, can be applied to measure surface velocity of a debris flows. In the case of debris flows the target for the measurement can be the front of a debris flow, a surface wave, a coarse particle or a piece of woody debris moving on the surface (Arattano and Marchi, 2008). Several other methods exist to measure surface velocity: spatial filter velocimetry (Itakura and Suwa, 1989), spatio-temporal derivative space method (Inaba et al., 1997), image processing techniques (see section 2.2).

The load of the debris-flow mass can be measured by installing load cells at the channel bottom (Genevois et al., 2000). If vertical and horizontal load cells are mounted on a force plate normal and shear stresses can also be measured (McArdell et al., 2007). As demonstrated in the Illgraben (McArdell et al., 2007), measuring normal stress in combination with the flow depth, is essential for the assessment of the mean bulk density of the flowing debris and its variation with time. Another parameter of the flowing debris, the pore fluid pressure, can be measured by installing pressure

transducers at the bottom of the channel (Berti and Simoni, 2005; McArdell et al., 2007).

An important debris-flow parameter that deserve to be measured for improving the design of debris-flow control works is the impact force. The impact force exerted by debris flows on obstacles along the path (e.g. buildings, check dams, defensive walls) can be measured by using pressure mark gauges installed on dam walls or large boulders (Okuda et al., 1980) or strain sensors (Zhang, 1993; Hu et al., 2011b), which allow continuous measurements.

Berger et al. (2011) constructed erosion sensor columns to monitor erosion depth and timing. A sensor column of a given length is composed of several cylindrical aluminum tubes, each of them containing an electronic resistor connected to the resistor of the overlying and underlying elements. When channel-bed erosion induced by a debris flow breaks the connection between one or more elements, a drop in total resistance occurs. This drop in total resistance, recorded on a data logger, can be related to the change in the length of the sensor column to determine the timing and the depth of erosion.

Finally, topographic surveys of debris-flow deposits (Figure 12) and variations in sediment sources and channel storage (Figure 13) deserve to be mentioned here as they permit comparison with debris-flow volumes assessed from debris-flow hydrographs (section 2.7). Topographic measurements and detection of geomorphic changes caused by debris flows can obviously be performed also in catchments not instrumented for the monitoring of debris-flow waves. They could thus be viewed as an approach to debris-flow monitoring complementary to systematic observations in catchments equipped with permanent devices: although limited to post-event volume assessment and geomorphic change detection, topography-oriented monitoring enables observations in a potentially large number of sites.

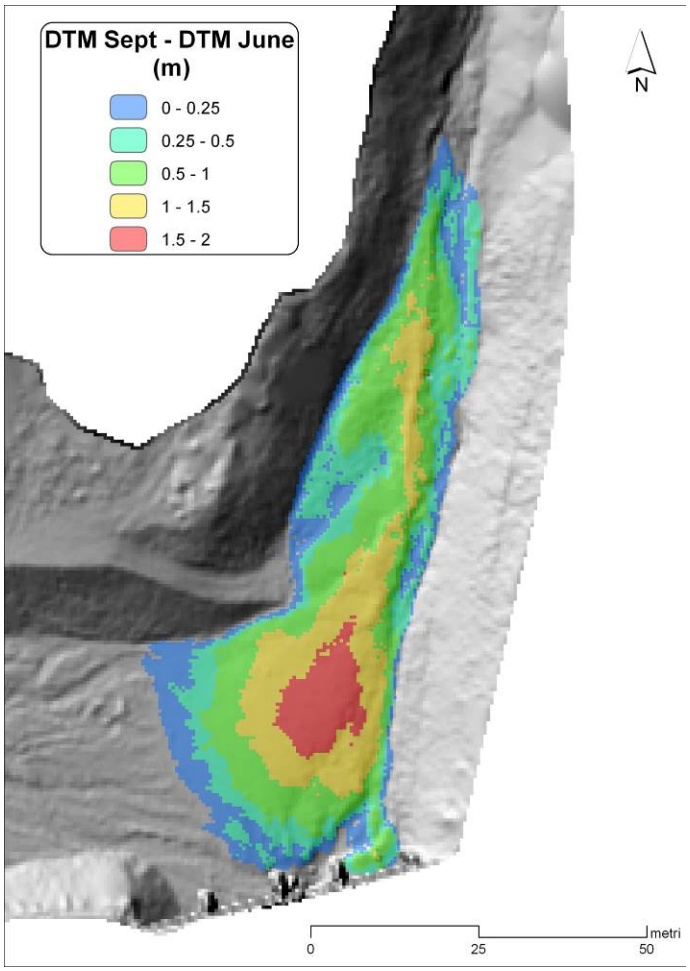

Figure 12 Map of sediment thickness deposited in the retention basin in the Gadria catchment (Italy) during a debris flow, evaluated as the difference between two TLS-derived DTMs

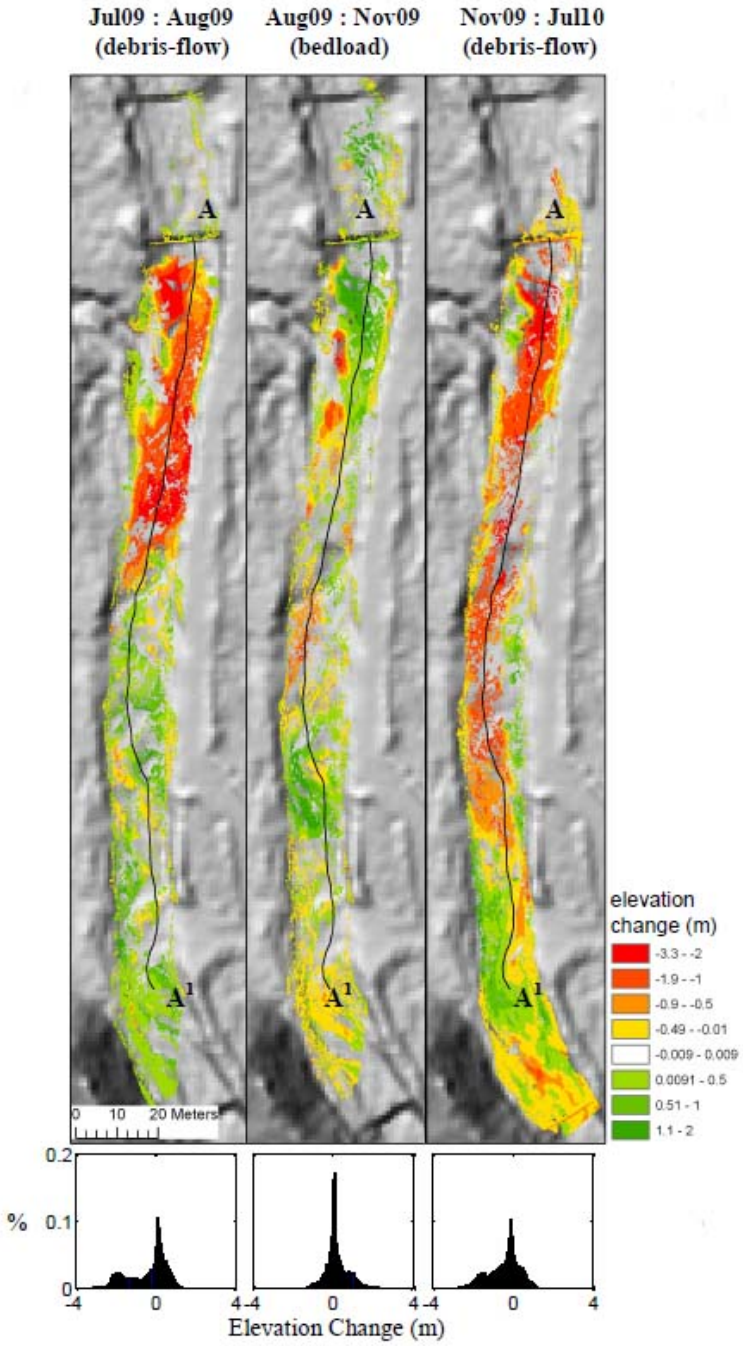

Figure 13 Topographic changes after debris-flow and bedload-transport events on a reach of the Manival Torrent from terrestrial laser scanning resurveys (Theule, 2012)

3 Suitability of debris-flow monitoring methods

In Table 3 are listed the suggested acquisition parameters for the main devices commonly applied for debris flow monitoring. Table 4 presents a classification in terms of suitability of debris-flow monitoring devices concerning specific parameters.

Table 3 Suggested acquisition parameters for different instruments used in debris flow monitoring

Instrument type	**Variable to monitor**	**Recording intervals**	**Other parameters/note**
Raingauge	Rainfall intensity/depth	1-5 min	0.2 mm bucket
Stage sensor	Flow depth	1-2 s	Radar sensors seem more reliable
Geophone	Ground velocity	1-2 s	Natural frequency of the sensor around 10 Hz Amplification factor: depending on the geology of the site and distance of the source
Videocamera	Flow images	8-10 fps	Image resolution depends on videcamera-flow distance and on the purpose (LSPIV vs simple flow description)
Load cell	Flow pressure and shear stress	1-2 s	
Laser-doppler speedometer	Surface velocity	1-2 s	
Piezometer	Pore-fluid pressure	1-2 s	

●●● highly suited for measuring this parameter

●● suited for measuring this parameter

● partially suited for measuring this parameter

not suited for measuring this parameter

Table 4 Suitability of debris-flow monitoring devices concerning specific parameters

Parameters of interest	Ultrasonic sensor	Radar sensor	Laser sensor	Geo-phone	Fiber optic sensor	Wire sensor	Pendulum	Micro-phone	Doppler speed-ometers	Video-camera
Debris-flow occurrence	●●●	●●●	●●●	●●●	●●●	●●●	●●●	●●●		●●●
Peak flow depth	●●●	●●●	●●			●				●
Debris flow "hydrograph"	●●●	●●●	●●●	●●	●●					
Ground vibration				●●●						
Mean flow velocity, peak discharge and volume	●●●	●●●	●●	●●●	●●			●●		●
Surface velocity									●●●	●●

4 References

Abancó C. Hürlimann M., Fritschi B.,Graf C. Moya J. (2012) - Transformation of Ground Vibration Signal for Debris-Flow Monitoring and Detection in Alarm Systems. Sensors,12, 4870-4891.

Arattano M. (1999) - On the use of seismic detectors as monitoring and warning systems for debris flows. Natural Hazards, 20(2-3): 197-213.

Arattano M., Deganutti A.M., Marchi L. (1997) - Debris flow monitoring activities in an instrumented watershed on the Italian Alps. Debris-Flow Hazards Mitigation: Mechanics, Prediction & Assessment: 506-515.

Arattano M., Marchi L. (2000) - Video-derived velocity distribution along a debris flow surge. Physics and Chemistry of the Earth part B, 25 (9): 781-784.

Arattano M., Marchi L. (2005) - Measurements of debris flow velocity through cross-correlation of instrumentation data. Natural Hazards and Earth System Sciences, 5(1): 137-142.

Arattano M., Marchi L. (2008) - Systems and sensors for debris-flow monitoring and warning. Sensors, 8(4): 2436-2452.

Aulitzky, H. (1989). The debris flows of Austria. Bulletin of the International Association of Engineering Geology, 40: 5-13.

Bacchini, M., Zannoni, A. (2003) - Relations between rainfall and triggering of debris-flow: case study of Cancia (Dolomites, Northeastern Italy). Natural Hazards and Earth System Science, 3(1-2): 71-79.

Badoux A., Graf C., Rhyner J., Kuntner R., McArdell B.W. (2009) - A debris-flow alarm system for the Alpine Illgraben catchment: design and performance. Natural Hazards, 49(3): 517-539.

Berger C., McArdell B.W., Schlunegger F. (2011) - Direct measurement of channel erosion by debris flows, Illgraben, Switzerland. Journal of Geophysical Research-Earth Surface, 116.

Berti M., Simoni A. (2005) - Experimental evidences and numerical modelling of debris flow initiated by channel runoff. Landslides, 2, 171-182.

Caine N. (1980) - The rainfall intensity–duration control of shallow landslides and debris flows. Geografiska Annaler, A, 62: 23–27.

Chang S.Y. (2003) - Evaluation of a system for detecting debris flows and warning road traffic at bridges susceptible to debris-flow hazard. Debris-Flow Hazards Mitigation: Mechanics, Prediction, and Assessment, Vols 1 and 2: 731-742.

Chou H.T., Cheung Y.L., Zhang S. (2007) - Calibration of infrasound monitoring system and acoustic characteristics of debris-flow movement by field studies. Debris-Flow Hazards Mitigation: Mechanics, Prediction, and Assessment, 571–580.

Coe J.A., Kinner D.A., Godt J.W. (2008) - Initiation conditions for debris flows generated by runoff at Chalk Cliffs, central Colorado. Geomorphology, 96(3-4): 270-297.

Genevois R., Galgaro A., Tecca P.R. (2001) - Image analysis for debris flow properties estimation. Phys. Chem. Earth (C), 26, 9, 623-631.

Genevois R., Tecca P.R., Berti M., Simoni A. (2000) – Debris flow in the Dolomites: Experimental data from a monitoring system. Proceedings of the Second International Conference on Debris-flow Hazards Mitigation: Mechanics, Prediction, and Assessment, Taipei, Wieczorek, G.; Naeser, N.; Eds.; A.A. Balkema, Rotterdam, 283-291.

Gomez C., Lavigne F. (2010) - Automated block detection in lahars through 3-bands spectral analysis of video images. Journal of Volcanology and Geothermal Research, 190, 379–384.

Guzzetti F., Peruccacci S., Rossi M., Stark C.P. (2008) - The rainfall intensity-duration control of shallow landslides and debris flows: an update. Landslides, 5(1): 3-17.

Hu K., Hu C., Li Y., Cui P. (2011a) - Characteristics and mechanism of debris-flow surges at Jiangjia Ravine. In: Genevois R., Hamilton D.L., and Prestininzi A. (eds), 5th International Conference on Debris-Flow Hazards Mitigation: Mechanics, Prediction and Assessment, Casa Editrice Università La Sapienza, Roma, pp 211-217.

Hu K., Wei F., Li Y. (2011b) Real-time measurement and preliminary analysis of debris-flow impact force at Jiangjia Ravine, China. Earth Surf. Process. Landforms 36, 1268–1278, DOI: 10.1002/esp.2155

Huang C.J., Yin H.Y., Chen C.Y., Yeh C.H., Wang C.L. (2007). Ground vibrations produced by rock motions and debris flows. Journal of Geophysical Research, 112, F02014, doi:10.1029/2005JF000437.

Huang C.-J., Chu, C.-R., Tien, T.-M., Yin H.-Y., Chen, P.-S. (2012) - Calibration and deployment of a Fiber-Optic Sensing system for monitoring debris flows. Sensors, 12 (5): 5835-5849.

Hungr O., Morgan G.C., Van Dine D.F., Lister R.D. (1987) - Debris flow defenses in British Columbia. In: Costa J.E. and Wieczorek G.F. (eds), Debris Flows / Avalanches: Process, Recognition, and Mitigation, Geological Society of America, Reviews in Engineering Geology, 7: 201-222.

Hürlimann M., Abancó C., Moya J., Raïmat C., Luis-Fonseca R. (2011) - Debris-flow monitoring stations in the Eastern Pyrenees. Description of instrumentation, first experiences and preliminary results. In: Genevois R., Hamilton D.L., and Prestininzi A. (eds), 5th International Conference on Debris-Flow Hazards Mitigation: Mechanics, Prediction and Assessment, Casa Editrice Università La Sapienza, Roma, pp 553–562.

Hürlimann M., Rickenmann D., Graf C. (2003) - Field and monitoring data of debris-flow events in the Swiss Alps. Canadian Geotechnical Journal, 40(1): 161-175.

Inaba H., Uddin M.S., Itakura Y., Kasahara M., 1997. Surface velocity vector field measurement of debris flow based on spatio-temporal derivative space method. Proceedings of the First International Conference

on Debris-flow Hazards Mitigation: Mechanics, Prediction, and Assessment, 757-766.

Itakura Y., Inaba, H., Sawada, T, 2005. A debris-flow monitoring devices and methods bibliography. Natural Hazards and Earth Systems Sciences, 5, 971-977.

Itakura, Y., Suwa, H., 1989. Measurement of surface velocity of debris flows by spatial filtering velocimetry. Proceedings of the Japan-China Symposium on Landslides and Debris Flows, Tokyo, 199-203.

Kogelnig A., Hübl J., Suriñach E., Vilajosana I., McArdell B. (2011) - Infrasound produced by debris flow: propagation and frequency content evolution. Natural Hazards, DOI 10.1007/s11069-011-9741-8.

Marchi L., Arattano M., Deganutti A.M. (2002) - Ten years of debris-flow monitoring in the Moscardo Torrent (Italian Alps). Geomorphology, 46(1-2): 1-17.

McArdell B.W., Bartelt P., Kowalski J. (2007) - Field observations of basal forces and fluid pore pressure in a debris flow. Geophysical Research Letters, 34(7).

McCoy S.W., Coe J.A., Kean J.W., Staley D.M., Wasklewicz T.A., Tucker G.E. (2011) - Observations of debris flows at Chalk Cliffs, Colorado, USA: part 1, in-situ measurements of flow dynamics, tracer particle movement and video imagery from the summer of 2009. In: Genevois R., Hamilton D.L., and Prestininzi A. (eds), 5th International Conference on Debris-Flow Hazards Mitigation: Mechanics, Prediction and Assessment, Casa Editrice Università La Sapienza, Roma, pp 715–724.

Muste M., Fujita I., Hauet A., 2008. Large-scale particle image velocimetry for measurements in riverine environments. Water Resources Research, 44, Doi 10.1029/2008wr006950.

Navratil O., Liébault F., Bellot H., Theule J., Travaglini E., Ravanat X., Ousset F., Laigle D., Segel V., Fiquet M., (2012) - High-frequency

monitoring of debris flows in the French Alps. Proc. 12th Interpraevent congress, Grenoble, 281-291.

Navratil O., Liébault F., Bellot H., Theule J., Ravanat X., Ousset F., Laigle D., Segel V., Fiquet, M., (2013a). Installation d'un suivi en continu des crues et laves torrentielles dans les Alpes françaises. Mémoires de la Société Vaudoise des Sciences Naturelles, 25: 83-97.

Navratil O., Liébault F., Bellot H., Travaglini E., Theule J.I., Chambon G., Laigle D., (2013b). High-frequency monitoring of debris-flow propagation along the Réal Torrent, Southern French Prealps. Geomorphology. DOI: 10.1016/j.geomorph.2013.06.017

Okuda S., Suwa H., Okunishi K., Yokoyama K., Nakano M. (1980) - Observations on the motion of a debris flow and its geomorphological effects. Zeitschrift für Geomorphologie., Suppl. Bd., 35: 142–163.

Pierson T. C. (1986) - Flow behavior of channelized debris flows, Mount St. Helens, Washington. In: Abrahms A. D. (ed), Hillslope Processes, Allen & Unwin, Boston, 269–296.

Suwa H., Okano K., Kanno T. (2011) - Forty years of debris flow monitoring at Kamikamihorizawa Creek, Mount Yakedake, Japan. In: Genevois R., Hamilton D.L., and Prestininzi A. (eds), 5th International Conference on Debris-Flow Hazards Mitigation: Mechanics, Prediction and Assessment, Casa Editrice Università La Sapienza, Roma, pp 605–613.

Tecca P.R., Galgaro A., Genevois R., Deganutti A.M. (2003) - Development of a remotely controlled debris flow monitoring system in the Dolomites (Acquabona, Italy). Hydrological Processes, 17(9): 1771-1784.

Theule J.I., 2012. Geomorphic study of sediment dynamics in active debris-flow catchments (French Alps), Unpublished PhD thesis, Université de Grenoble, Grenoble, 152 pp.

Wilson R. C., Mark R. K., Barbato G. (1993) - Operation of a Real-time warning system for debris flows in the S. Francisco Bay Area, California. In:

Hsieh Wen Shen, S. T. Su e Feng Wen (eds), Hydraulic Engineering '93 vol. 2, ASCE 1993 National Conference on Hydraulic Engineering and International Symposium on Engineering Hydrology, American Society of Civil Engineers, New York, pp 1592-1597.

Yin H.-Y. (2012) Debris-flow monitoring and warning in Taiwan. International workshop “Monitoring bedload and debris flows in mountain basins”, Bolzano – Bozen (Italy), October 10-12, 2012

Yin H.-Y., Huang C. J., Chen C. Y., Fang Y. M., Lee, B. J., Chou, T. Y. (2011) - The present development of debris flow monitoring technology in Taiwan – A case study presentation. In: Genevois R., Hamilton D.L., and Prestininzi A. (eds), 5th International Conference on Debris-Flow Hazards Mitigation: Mechanics, Prediction and Assessment, Casa Editrice Università La Sapienza, Roma, pp 623–631.

Zhang S. (1993) - A Comprehensive Approach to the Observation and Prevention of Debris Flows in China. Natural Hazards, 7(1): 1-23.

Zhang S., Chen J. (2003) - Measurement of debris-flow surface characteristics through close-range photogrammetry. In: Rickenmann D, Chen C-L (eds) Debris-flow hazards mitigation: mechanics, prediction, and assessment. Proceedings of the third international conference. Millpress, Rotterdam: 775–784.

Zhang S., Hong Y., Yu B. (2004) - Detecting infrasound emission of debris flow for warning purposes. Internationales Symposium Interpraevent VII: 359–364

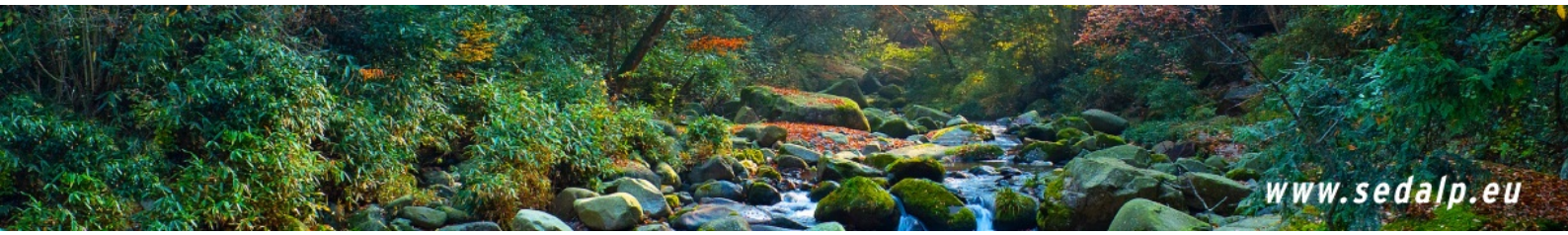

Part III

Protocol for Wood Monitoring

WP5 - Action 5.2

Protocols on standardized data collection methods in sediment transport monitoring for transboundary exchange

Lead authors:

Hervé Piegay (PP8)

Contributors:

Mario Aristide Lenzi, Lorenzo Picco

& Diego Ravazzolo (all PP03)

June, 2013

Contents

Introduction

Large wood is an important component of river systems, because it contributes to many different processes as geomorphic, hydraulic, and ecological (Brookes, 1988; Gurnell et al., 2002; Sedell et al., 1988). On the other side, wood in-channel transported during flood events could be a problem for some human activities on rivers as, for example, commercial marine operations on large rivers (Gurnell et al., 2002; Piégay, 2003). It represents a risk for flooding and human infrastructure (Bradley et al. 2005, Comiti et al. 2006), notably when it accumulates on or near to sensible structures as bridge piers (Wallerstein, 1998; Kothyari and Ranga Raju, 2001). Wood in rivers can be an obstacle for flows during floods, exacerbating locally flooding and infrastructure damages.

There is a need for data to calibrate wood budgets and examine processes related to the transport of wood during floods (Benda and Sias 2003, Hassan et al. 2005). Previous studies of wood in rivers have quantified spatial distributions but temporal dynamics remain poorly documented. The lack of such data is related to limitations inherent in existing methods, especially when applied to large rivers.

For these reasons, and also for a better management of the river system, it is important to understand where the wood is recruited, moves and where it tends to accumulate system (Curran, 2010). However, the dynamic and mobility of large wood in rivers is poorly understood, especially in wide gravel-bed rivers. There is still a considerable lack of knowledge on the complex set of processes involved in the recruitment, transport and deposition of woody elements all over the fluvial systems. Even more on the quantification of these processes at the range of spatial and temporal scales at which they occurred. Only a few studies focused on this kind of surveys, requiring a lot of time (Table 1).

Large wood (LW) can be defined as the woody elements (including roots and branches) characterized by 1 m or more of length and diameter greater than 0.1 m or both (Jackson and Sturm, 2002).

Five existing technologies were field-tested by MacVicar et al. (2008) to assess their utility for quantifying the temporal dynamics in rivers: passive Radio Frequency Identification (RFID) transponders, Active RFID transponders, radio transmitters, video monitoring, repeated high-resolution aerial photos (produced by a low-flying drone aircraft). Passive RFID transponders and radio transmitters are reliable for wood tracking. Radio transmitters are suited to multi-year (~ 5 year) surveys and can be detected at 800 m, whereas passive RFID transponders are limited by a read range of 0.30 m but suited for longer term studies. Active RFID transponders combine a moderate read range (With an antenna) and low cost with the ability to monitor wood transport during floods but require more testing. Video monitoring is used to monitor the wood passage within a given section.

Amongst these 5 technologies, 2 are detailed here (RFID tracking and video) and a new one is available based on GPS tracking.

Table 1 Summary of previous field studies of wood movement and wood deposit renewal in river

Reference	Techniques	Type of survey	River	Drainage Area (km^2)	Survey dist-ance (km)	Study dura-tion (yr)	n	Reco-very (%)
Lienkaemper and Swanson (1987)	Field survey – visual	Key pieces, unlogged	Mack Creek	6.0	0.11	1 flood	42	100[a]
Bilby (1984)	Field survey – numbered tags	Post logging	Salmon Creek	9.0	1.10	0.5	74	~80 in first flood
Keim et al. (2000)	Field survey – numbered tags	key pieces post logging	Bark, Buttermilk, and Hudson Creeks	7.0 – 15.6	0.45 – 0.70	3	21	76
Haga et al. (2002)	Field survey – numbered tags	Uniform 1.6 m long pieces	Oyabu Creek	5.3	5.5	1	63	95 in first flood
Jacobson et al. (1999)	Field survey - numbered tags	In-situ wood, ephemeral stream	Kuiseb River	14,700	160	1 flood	2105	21
Andreoli et al (2007)	Field survey – numbered tags	All wood > 0.1 m diameter	2 mountain basins of Southerns Andes	9 - 13	1.5 – 1.8	1	322 - 381	98 - 100
Piégay and Marston (1998)	Field survey	Channel bank	Ain River	3,630	point	3	1 jam	-
Van der Nat et al. (2003)	Field survey	In-channel wood	Tagliamento River	2,580	4	2	random locations in 2 reaches	-
Haschenburger and Rice (2004)	Aerial	Jams only	Carnation Creek	11	3	7	5 jams	-
Lassettre et al. (2007)	Aerial	Helicopter photograph	Ain River	3,760	40	10	445 – 1008	-
Moulin and Piégay (2004)	Point survey - reservoir	All transported wood	Rhône River	10,910	point	10	13,000 m^3/yr[b]	100
Seo et al. (2008)	Point survey - reservoir	All transported wood	131 reservoirs in Japan	6.2 – 2,370	point	1–29	300 – 400,000 kgC/yr[c]	100

Notes a) Transported wood was stopped in downstream reservoir

b) Volume of wood trapped in reservoir.

c) Volume of wood trapped in reservoir converted into mass of carbon.

1 Wood tracking devices and methods

This protocol focuses on the devices used for monitoring the mobility and displacement of LW during and after flood events. We also present the methods commonly employed to measure the most relevant parameters for LW investigations.

It is known that in wide rivers, there are some problems to survey the LW along the entire active channel area. This is the reason because it is necessary to adopt a sampling procedure identifying cross-sectional transects which limit the reliability of LW storage (Gurnell et al., 2000a; 2000b). Field surveys can be carried out using the guideline of a spread sheet to measure different characteristics such as, for example, the state of decay, orientation to flow and position in the channel (Table 2).

Volume of LW is identified through its mid-diameter and length measured using tree caliper and tape, respectively (Mao et al., 2008). Log mobility and displacement during and after flood events can be measured applying two monitoring techniques: implanting radio frequency identification (RFID) tags in logs (McVicar et al., 2009) and using GPS Track devices.

Table 2 Example of spread sheet guidelines for LW survey

Type		K= (*key*), R= (*racked*), L= (*loose*)			
ID					
GPS Position	N		E		
Characteristics					
Tipologia		**Branches**		**Roots** (Y/N)	
Tree		total absent		entire rootwad	
Shrub		some broken branches		Diameter (m)	
Trunk		all branches intact		Length (m)	
				Presence portion of fine roots	
State of decay		**Origin**		**Size**	
intact with bark		natural mortality			
intact without bark		bank erosion		**Trunk**	
porous		transport, fluitation		Diameter (m)	
decaying				Length (m)	
bark (%)		**Orientation**			
		upstream rootwad		**Tree**	
Vegetative activity (leaves)		downstream rootwad		width (m)	
Absent		rootwad (Dx/Sx)		length (m)	
Before the fall		° resp. the North		high (m)	
After the fall		° resp. The flow direction			
Position	**In section**			**In plan**	
Thalweg (A1)				lateral bar	
Shallow (A2)				longitudinal bar	
Chute channel (A2, B1)					
Active bar (B1)					
High bar (B2)					
Berm/bench/shelf (B2)		**Vegetation**		**Channel**	
Secondary channel (B2, C)		veg. herbaceous / shrub		step	
Pioneer island (B2, C)		veg. (2-5 anni)		riffle	
Established island (B2, C)		veg. (>5 anni)		pool	
Floodplain (C)					
Terrace (D)					
Interactions wood - flow					
completely submerged		*underflow*		deviation of the flow	
partially submerged		depth of underflow (cm)		contraction of the flow	
Interactions wood - sediments					
upstream		**on the trunk / accumulation**		**downstream**	
deposition		partially buried		deposition	
scour		entirely buried		scour	
lateral deposition (*Dx/Sx*)				lateral deposition (*Dx/Sx*)	
lateral scour (*Dx/Sx*)				lateral scour (*Dx/Sx*)	
length (m)				length (m)	
width (m)				width (m)	
high/depth (m)				high/depth (m)	
fine woody		fine woody		fine woody	
fine sediment		fine sediment		fine sediment	
sand		sand		sand	
gravel		gravel		gravel	
Note					

1.1 Wood tracking using RFID

Pa*ssive Radio Frequency Identification (RFID) transponders*, originally developed for security and commercial purposes, also known as Passive Integrated Transponder (PIT) tags, have previously been applied to track the movements of fish (Feldheim et al., 2002) and sediment particles (Lamarre et al., 2005) in rivers. RFID technology uses electromagnetic coupling to transmit an identification code as 'noise' on a radio frequency signal. This code is unique to each tag, while the transmission frequency is shared. Passive RFID transponders are transponders, which means that they transmit a signal in response to an incoming signal. The energy used to transmit the signal is taken from the received signal, and the tags do not have batteries. While a range of transponder shapes and sizes are commercially-available, this study used a hermetically sealed 23 x 4 mm glass cylinder transponder (Figure 1) transmitting at (134.2 kHz) that was developed by TIRIS Technology. The tags are detected using a portable control unit and antenna. Key advantages of these tags are that they can be programmed with unique identification codes, which allows a precise spatial analysis of wood mobilisation and deposition; the durability of the tags in extreme environments; and the lack of a battery, which allows long term studies. An important limitation of the technique is that the detection range is only about 30 cm for the tag and antenna combination that was used in this study.

Figure 1 Example of passive RFID tag of TIRIS Technology composed by 23.4 mm glass cylinder transponder transmitting at (134•2 kHz).

Active RFID transponders are similar to passive RFID transponders in that they use electromagnetic coupling on a shared radio frequency to allow the remote identification of unique tags. Active RFID transponders are transmitters, however, and they emit a beacon signal at a predetermined time interval. While a range of tags are available from different companies, this study utilized 433 MHz tags purchased from RFCode Inc. Each tag is enclosed in a shock and splash-resistant polycarbonate case that is 47 x 34 x 12 mm in size (Figure 2). They use a replaceable coin cell battery. Fixed and mobile readers are available so that the techniques allowed to survey wood deposit and mobilisation as well as wood input from floodplain but also censing the wood output from the study reach (Q_0) which is was not possible with the previous tracking techniques so that it is not possible to know if wood piece disappeared because the signal is not captured or because they moved away. The mobile reader can be clipped onto a belt and communicates via Bluetooth™ to a handheld computer. A significant advantage of this technique is that the detection range with the fixed reader (~300m) is sufficient to detect tags from a streamside station in many rivers. The principal disadvantage is that the signal transmission requires batteries, which limits the lifetime of the tag. These tags have not previously been tested in rivers.

Figure 2 Example of active RFID tag are those of the company RFCode Inc in which each tag is enclosed in shock resistant and splash resistant case that is 47-34-12 mm in size.

Both mobile and fixed readers are available. We installed the software supplied with the mobile reader by RFCode on a Trimble GeoXT Handheld GPS. A fixed reader was installed at a gauging station. A Tavis data router was connected to the reader and equipped with a memory card to record the identification codes of detected trees and their time of passage. Two Yagi antennae were installed on a pole outside of the station pointed across and upstream on the river. The gauging station is equipped with electrical and telephone connections.

1.2 GPS Track

This technique of LW monitoring has never been tested before in rivers monitoring activities, consents to record the displacement of a log during a flood event using a GPS track devices (passive or active). The aspect that distinguishes the active from a passive GPS track is the capacity to send, in real time, Short Message Service (SMS) over GSM communications network (i.e. time, position, batteries lifetime).

An example of active GPS track device is the Trim Trac Locator by Trimble (Figure 3). This GPS track has dimensions of 143 mm x 76 mm x 38 mm and weight of 205 grams (not including batteries). The device work with 4 AA batteries which permit to operate up to 90 days under typical usage with good GPS signal strength. The device is composed by an internal GPS antenna and it has a cold start GPS acquisition time, warm start and hot start GPS of <90, ~50 and <24 seconds respectively. During the displacement the device has an internal flash data storage capacity of 1026 GPS positions (1 GPS position every 10 s). The Trim Trac Locator is not waterproof but only water-resistant and tested to IP-55, for this reason it is necessary to waterproof each GPS Track using a plastic box and seal it with silicon. It is, also, necessary to place into the box a RFID in order to allow post-event recovery in case of exhausted batteries. Plastic boxes were fixed to woody elements tying them to the trunk with metal chains and cable ties, 50cm high from the base of the trunk.

Figure 3 Trimble Trim Trac locator, an example of GPS Track device

During the monitoring period it is important to do a good maintenance to the batteries and to the correct waterproofing of the plastic box.

Post-event it is possible to identify the position of the logs with the GPS track through the last SMS sent and using the mobile reader to recognize the RFID placed into the plastic box. The Differential Global Positioning system (DGPS) is needed for each logs with GPS track installed, before and after every flood event.

2 Wood passage censing using video monitoring

Existing methods that use tagging or repeat surveys of stored wood volumes are ineffective and labour intensive in large rivers and do not monitor the transport or accumulation of wood during floods when access to the river is

most hazardous (Lyn et al. 2003, Moulin and Piégay 2004, MacVicar et al. 2009).

There are an increasing number of commercially-available video camera and software packages. With access to the internet, the data can be stored off site, which reduces the requirements of the on-site computer system. The advantage of the video technique is the ability to detect and measure wood passing on the water surface of a river in a remote location. The primary limitations relate to image resolution and the oblique angle of the camera, which means that water surface reflections are an issue and that image resolution is not constant over the width of the channel.

The present report provides feedbacks on an Axis 221 Day/Night ™ camera with an infrared mode. A first video camera has been installed in the spring of 2007 at the gauging station at Pont de Chazey on the Ain River. The camera is set at an angle such that it has a view of the entire river width. It is located on the side of the river closest to the thalweg to provide a maximum resolution where the majority of wood is expected to pass. We installed a Profiline™ infrared light projector (model number TV6899) to increase luminosity at night. This type of camera was selected because of the low-light sensitivity and the quality of the video. Using software developed by the security services company Innovatys (France), videos are transferred to remote servers. Fifteen minute segments use approximately 94 Mb of memory when saved in *.mjpg format at 5 frames per second and minimum compression. A 300 Gb hard drive is sufficient for approximately 30 days of video. Visual detection is limited to the wood that can be clearly identified on a recorded image. To test the significance of image resolution errors for wood detection, the water surface was monitored at four positions across the width of the channel from the upstream bridge (central pier is visible in upper left corner of image) during the rising limb of the flood on November 23, 2007. Despite attempts to use infra-red illumination, it was not possible to reliably identify and measure floating wood at night. Noted problems at night were the incomplete coverage of the

field-of-view by the infra-red illumination and a camera algorithm that decreased the shutter speed to allow for sufficient light to reach the sensor, resulting in blurred objects. .

2.1 Semi-manual detection of wood

A semi-manual logging algorithm created in Matlab™ records the position, velocity, dimensions, and other details about detected wood pieces in the video (Figure 4). Method is described in MacVicar et Piégay (2012). This algorithm advances the video one frame at a time. When wood is visible, the user manually locates the endpoints and edges of the trunk. The time is then read from the image, and the coordinates of the wood are transformed using a rectification algorithm to obtain the length and diameter of the wood and its position and angle relative to the banks. The rectification algorithm was calculated by measuring ground control points during low flow using a total station and transforming the image as described below. The presence/absence of roots, branches and leaves are noted for each wood piece. The video is advanced until the user stops the video and locates the endpoints a second time. The downstream and angular velocities are then calculated. Velocity and angular velocity are calculated from the difference in position and time between two recorded images.

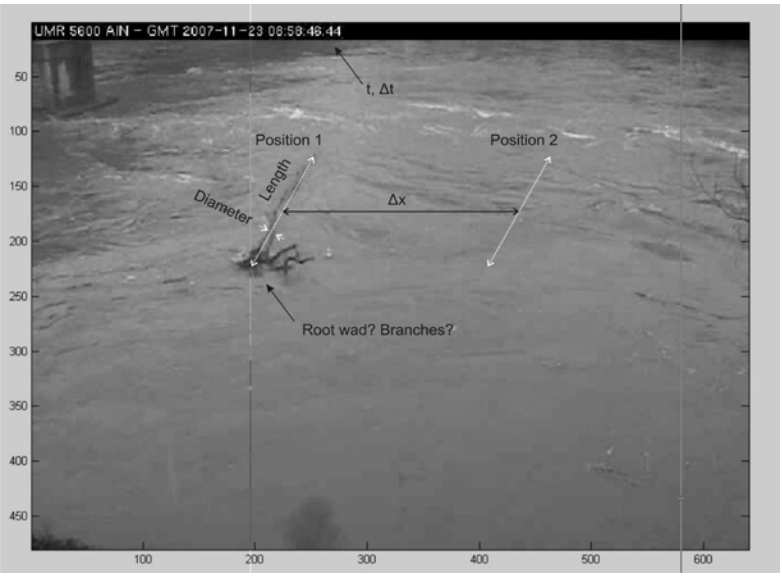

Figure 4 A grayscale video frame from the camera on the Ain River. A piece of floating wood is shown at Position 1. The length, diameter, and position 2 of the wood piece are shown to demonstrate the calculation of wood volume and velocity from the semi-manual image analysis procedure.

2.2 Wood volume calculation

Ground-based cameras have an oblique view angle (Figure 5a), which means that pixel size is variable and distortion can be an important effect (Hauet et al. 2008a). As a general rule, images are ortho-rectified prior to analysis. Ortho-rectification refers to the process by which image distortion is removed and the image scale is adjusted to match the actual scale of the water surface (Figure 5b-c) Ortho-rectification is accomplished by applying an appropriate image photogrammetric transformation (Mikhail and Ackermann 1976) using known coordinates of ground control points (GCPs) in the real (*X*, *Y*, and *Z*) and the image (*x* and *y*) coordinate systems. The mapping relationships between the two systems can be expressed as (Fujita et al. 1998):

$$X = \frac{L_1 x + L_2 y + L_3 z + L_4}{L_9 x + L_{10} y + L_{11} z + 1} \qquad (1a)$$

$$Y = \frac{L_5 x + L_6 y + L_7 z + L_8}{L_9 x + L_{10} y + L_{11} z + 1} \qquad (1b)$$

where the eleven mapping coefficients L_1-L_{11} can be determined by the least square method using the known GCPs coordinates. A minimum of 6 GCPs are needed for conducting the transformation. While more GCPs are useful for checking errors in survey data, the uncertainty caused by pixel size is usually greater than that caused by survey error, and additional points are not necessary for the analysis (Bradley et al. 2002). Fewer points can be used if the image coordinates are assumed to be on the same vertical plane. The size of the non-distorted image should be nearly the same as that of the original image. In addition, a reconstruction of the pixel intensity distribution is made to obtain the ortho-rectified image. Following Muste et al (1999), intensity at a pixel in the transformed image is obtained using a cubic convolution interpolation of the intensity in 16 neighboring pixels of the original image.

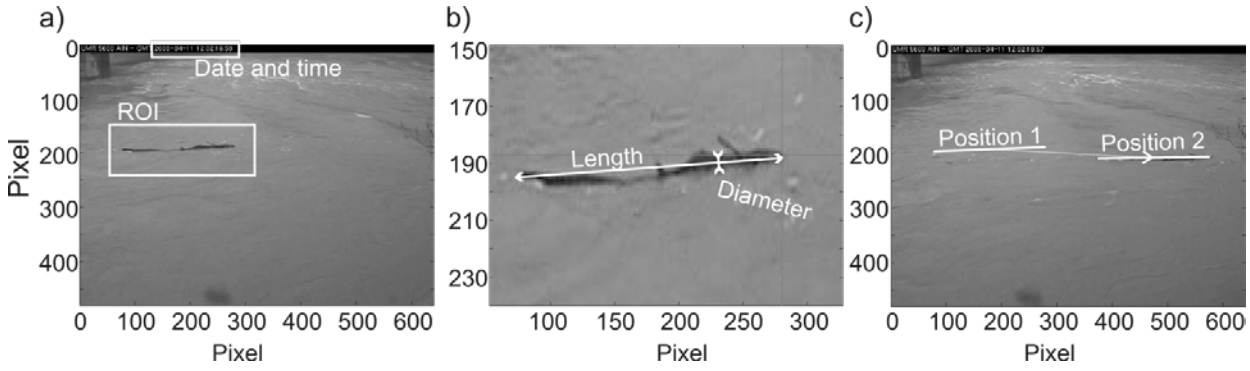

Figure 5 Wood detection procedure showing a) definition of a region of interest (ROI) based on a visual detection of wood including measurement of date and time from time stamp b) precise location of end and side points to define the piece length, diameter, and first position; and c) definition of second position after advancing a user-determined number of frames to allow calculation of velocity and angular velocity.

A geometrical correction is then applied to the transformation using water elevation data from the gauging station and the known position of the camera to account for effect of the rise in water elevation with discharge (Figure 6).

The water surface correction improves the accuracy of *L* and *D* estimates from the video over what was presented by MacVicar et al. (2009). Without the correction, which compensates for the fact that wood is closer to the camera as flood stage increases, small wood can be misclassified as large wood (L ≥ 0.10 m) and volume estimates of all wood pieces are too high. When the correction was applied to the videos analysed by MacVicar et al. (2009), it was found that 48% of small wood pieces had been erroneously classified as large wood, and the revised estimated of wood transport was only 30% of the previously estimated volume.

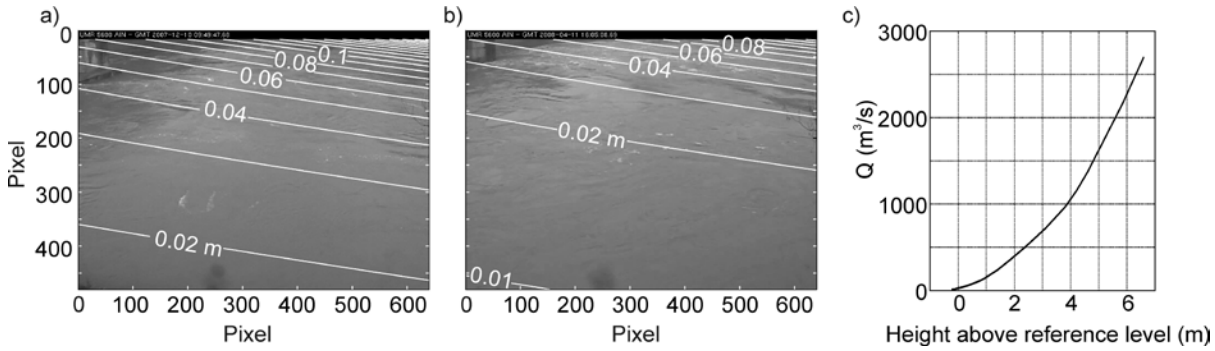

Figure 6 Image resolution as a function of discharge (Q). a) pixel size contours at low flow (0 m above reference level), b) pixel size contours at high flow (4 m above reference level), and c) the gauge relation between height above reference level and discharge.

2.3 Actual limitations and error estimate

Detection of wood on frames is still manual

Wood transport measurements were only made from selected sample periods in the continuous video record due to the laborious nature of the measurement procedure. The minimum sampling frequency was one 15 min video segment every 2 hours during the daylight hours over the duration of significant wood transport. Sampled videos were evenly spaced over the flood duration with two exceptions. First, the frequency was increased to one 15 min video segment per hour when tested discharge was between 400 and 600 m^3/s during rising limbs. This range was the only one that was common to all three floods, and was used to compare inter-flood variability. Second, one entire hour was sampled during the rising limb of the APR08 flood (Q ~ 800 to 900 m^3/s) to better assess the variability of wood transport during above bankfull stages. Overall between 5 and 9% of the total flood was sampled for the three floods.

Estimate of wood diameter

Sources of error were related to the difficulty of assessing wood diameter and the inability to detect and measure wood in certain cases. The assumption of straight cylinders was felt to be a reasonable simplification of the wood carried in transport given the dominance of large diameter poplar species in the floodplain, which typically have straight trunks with few large branches. Diameter was measured near the midpoint of the trunk so that an approximately average diameter was used. In general it should be noted that the diameter measurement from imagery is more sensitive than the length measurement due to its relatively smaller value, even when wood is measured on dry bars (MacVicar et al. 2009). Given that the wood here is floating in the water at an oblique angle to the camera, it is likely that diameter measurements contain significant and unavoidable error.

Wood in transport below the water surface and in groups was additional problems (Figure 7). Figure 7b shows one frame from a case in which the branches turned vertically in a manner that suggested that the non-visible end of the wood piece was in contact with the channel bed. Some wood may have neutral or negative buoyancy due to the retention of rock and soil in root wads and the higher water content of recently eroded wood. The transport of wood in groups can also result in significant submerged wood (Figure 7c) and is difficult to isolate and measure all of the significant wood pieces in these cases.

Figure 7 Sources of error a) poor visibility at night (including a spider top right); b) submerged wood (visible branches turned vertically in the frame); and c) floating wood jams with uncertain configuration.

2.4 Perspectives in automatic detection of wood

An application allowing the detection of floating pieces of wood in rivers from a video file, which is obtained thanks to a webcam in a static position, in *.avi* or *.mjpg* format is in development in the project.

The software outputs a list of the detected wood blocks in an *xml* or a *yaml* file. This list comprehends the position of wood blocks in each image where they were detected, their bounding boxes' coordinates and size (as a number of pixels) in the image, and the frame time data when available. The software can output a capture of their corresponding video frame, an image of their binary

mask and/or their probability mask, depending on the configuration set by the user.

The software can also be configured thanks to configuration files, which can be simply and quickly modified with the help of a simple text editor.

For now, this application has only been tested under MS Windows (XP and 7), provided the free OpenCV library is already installed. It runs in command-line. With a 4 cores 3 Ghz Intel processor with 4 GB of RAM, it currently takes approximately 2 minutes to analyze 15 minutes of video.

Algorithmically, the software uses a combination of several probability maps to determine the presence of wood in an image. A first map is computed on each frame statically, based on intensity and/or color information. A second map is computed dynamically, based on the change of pixels intensity between consecutive frames. Both maps are combined, and a threshold is used to extract connex components from each frames. Those connex components are then analyzed in order to regroup them or reject them as plausible wood blocks. This algorithm is detailed in [1].

[1]Object Detection in Dynamic Background, Imtiaz Ali, Thèse de l'université de Lyon, 2012

Seven video segments (total duration of 36 minutes) were used to develop the algorithm to detect and count wood objects on the surface of the river. This algorithm was developed by breaking the larger problem into three tasks: 1) detection and recognition of objects on water surface (image segmentation); 2) agglomeration of objects in close proximity into a single object; and 3) distinction between wood and other types of objects such as water waves (Ali and Tougne 2009)(Figure 8).

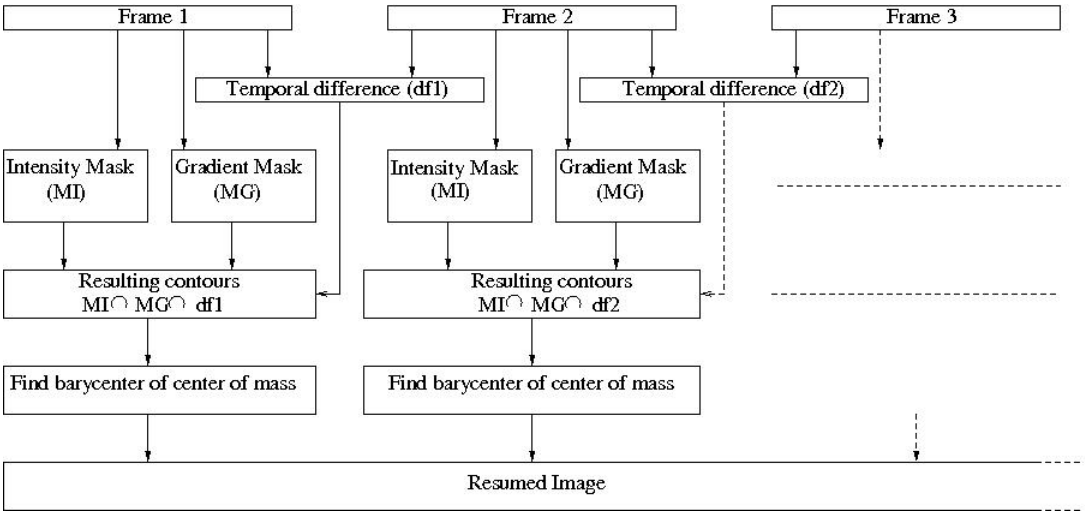

Figure 8 Image analysis procedure for identification of floating wood from video imagery.

Histogram thresholding is among the most popular techniques for identifying objects (segmentation) in gray-level images (Fu and Mui 1981, Pal and Pal 1993). Using this technique, histograms of the gray-level image intensity are calculated and regions with similar values are identified as objects or regions within the image. The Fisher linear discriminate technique, a standard method used in statistics for data clustering and pattern recognition, was applied to distinguish intensity clusters and obtain a intensity mask (MI) of objects or regions in each image frame (Haralick and Shapiro 1985, Jain et al. 1995). This technique produced very good segmentation of images and identification of regions in the absence of direct sunshine (Example 1, Figure 9b) but was compromised by shadows on the water surface (Example 2, Figure 9b). In addition, water waves frequently had similar intensity values to wood, resulting in classification errors.

Due to possible errors associated with histogram thresholding, it was necessary to integrate spatial features of the image with spectral features. For this reason, images were also analysed using an edge-detection algorithm in which the local gradients in image-intensity values were used to define boundaries between regions within the image (Chapron 1997, Zugaj and Lattuati 1998, Zhao 2008). The resulting image is called a gradient mask (MG) and is

obtained for each image frame (Figure 9c). The advantage of a gradient mask is that it can be used to detect objects even when illumination is not constant over the entire image due to shadows from trees and the bridge. However, due to the roughness of the water surface, both water waves and wood have strong gradients in intensity values, and a large number of false detections occur if this method is used exclusively.

To reduce the number of false detections, an additional mask was calculated from the temporal difference between two consecutive frames (df). This mask was applied based on the principle that wood will be present in consecutive video frames while the majority of water waves will be stationary or dispersed between images. A final segmented image was calculated from the intersection of the intensity mask (MI), the gradient mask (MG), and temporal inter-frame difference (df). This final image is a binary matrix that identifies all detected objects within the frame (Figure 9d).

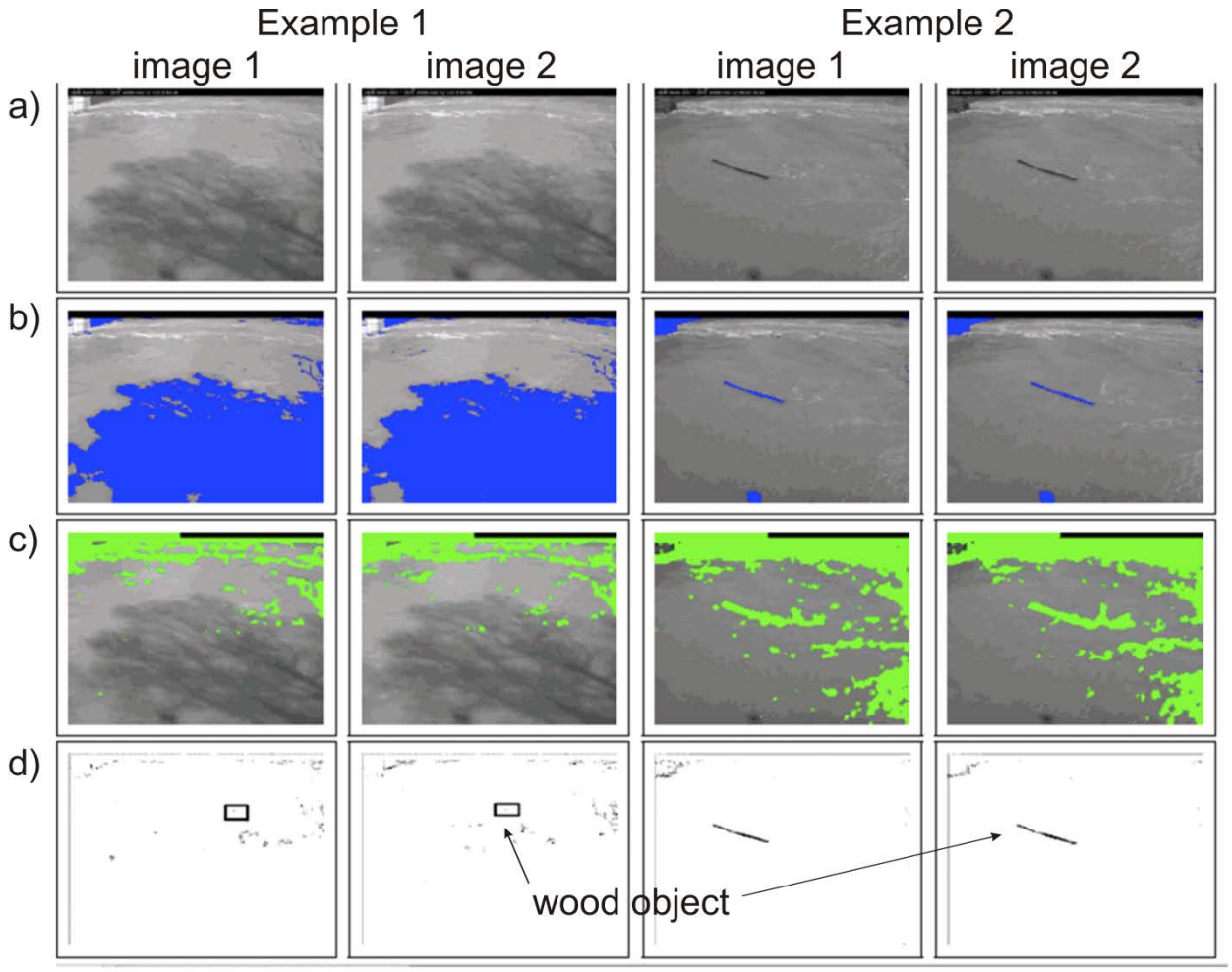

Figure 9 Image segmentation steps involved in floating wood identification procedure for a small object in shadows (Example 1) and a larger object in sunlight: a) original images, b) intensity masks, c) gradient masks, and d) resulting combinations of all segmentations.

An additional problem from the image segmentation procedure is that not all of the detected objects are distinct. For example, a single wood object can be made of a number of parts such as roots and branches. Part of the trunk may be submerged, resulting in the appearance of distinct objects. In addition, the size and shape of wood objects can change from one frame to the next due to water waves and the motion of the wood. Multiple objects identified in the image segmentation must be grouped together to match real objects and avoid false detections. This was accomplished by calculating the distances between all object centroids in an image and grouping close objects and calculating their

'meta-centroid' based on a criterion for the minimum distance between centroids.

Despite the use of the temporal difference mask to reduce false detections, a number of water waves were present and in motion for consecutive frames. To distinguish between wood and water waves it was necessary to utilize some additional property of the wood. Given that water travels from left to right in the image frame, it was reasoned that wood must also travel in the same direction while the direction of wave propagation will be more random and would tend to disappear over time. To track the movements of objects, their meta-centroids were represented at each time step in a summary image. A multi-segment vector was formed in the summary image due to the movement of objects in a series of frames. The algorithm distinguished wood objects as those for which the meta-centroids were present in a number of consecutive images and moved continuously from left to right. Parameters were tested for different type lighting situations and different length of wood objects. It was determined that the optimum number of consecutive images to distinguish wood objects from waves was five images, or a total time of 1 second for the video recording at 5 Hz.

A first comparison of the number of detected wood (N_d) to the number of wood pieces identified from the manual analysis of the video (N) show that there is an approximately 90% agreement between the two methods. An additional 8% of wood pieces were detected with the algorithm but were not counted because they were not present for five consecutive frames in the video. Some floating wood pieces sometimes disappear for one or two frames as they bob slightly at the surface or momentarily reflect the light. Such types of wood pieces are difficult to count accurately using the current method. Acomparison of the number of missed detections of wood (N_{md}) and the number of false detections of wood (N_{fd}) shows that these errors are in the range of 10 to 15% (Table 3 Quantitative evaluation of proposed algorithm comparing the number visually detected wood pieces (N) to the number that were detected using the computer

algorithm (N_d), the number of wood pieces that were missed by the algorithm (N_{md}), and the number of false detections made by the algorithm (N_{fd}).). False detections occur due to occasional water waves that last more than five consecutive frames, while missed detections occur because the intensity of wood pieces can be very close to that of the water.

Table 3 Quantitative evaluation of proposed algorithm comparing the number visually detected wood pieces (N) to the number that were detected using the computer algorithm (N_d), the number of wood pieces that were missed by the algorithm (N_{md}), and the number of false detections made by the algorithm (N_{fd}).

Video	Total frames	Manual Detected	Algorithm Detected		Missed Detections		False Detections	
		N	N_d	%	N_{md}	%	N_{fd}	%
1	650	82	78	95	4	5	5	6
2	900	73	67	92	6	8	22	30
3	860	21	17	81	4	19	4	19
4	750	40	36	90	4	10	3	8
5	550	38	29	76	9	24	1	3
6	800	28	26	93	2	7	8	29
7	880	36	33	92	3	8	7	19
Total	5390	318	286	90	32	10	50	16

3 Suitability of wood monitoring methods

Table 4 presents a classification in terms of suitability of wood monitoring devices concerning specific parameters. The point classification is as follows:

●●● highly suited for measuring this parameter

●● suited for measuring this parameter

● partially suited for measuring this parameter

not suited for measuring this parameter

Table 4: Suitability of wood monitoring devices concerning specific parameters

Parameters of Interest	GPS	RFID (Passive Radio Frequency Identification)	Video censing
Wood discharge estimate			●●●
Displacement length	●●●	●●●	
Location of preferential sites of deposit	●●	●●	
Entrainment discharges of wood	●●	●●	
Wood budgeting (in channel storage)	●●	●●	
Wood budgeting (output)			●●
Flow conditions (water depth, width, velocity)			●●

References

Ali, I., and L. Tougne (2009), Unsupervised video analysis for counting of wood in river during floods, in Conference Proceedings of *5th International Symposium on Visual Computing,* 578-586, Springer, Las Vegas, USA.

Bocchiola, D., M. C. Rulli, and R. Rosso (2006a), Flume experiments on wood entrainment in rivers, *Advances in Water Resources*, 29, 1182-1195.

Bocchiola, D., M. C. Rulli, and R. Rosso (2006b), Transport of large woody debris in the presence of obstacles, *Geomorphology*, 76, 166-178.

Braudrick, C. A., and G. E. Grant (2000), When do logs move in rivers?, *Water Resources Research*, *36*, 571-583.

Braudrick, C. A., and G. E. Grant (2001), Transport and deposition of large woody debris in streams: a flume experiment, *Geomorphology*, 41, 263-283.

Brookes, A. (1988) Channelized rivers; perspectives for environmental management. John Wiley & Sons, Chichester.

Curran J.C., (2010). Mobility of large woody debris (LWD) jams in a low gradient channel. Geomorphology 116 (3–4), 320–329

Comiti, F., E. Pecorari, L. Mao, L. Picco, E. Rigon, M.A. Lenzi M.A. (2008b) New methods for determining wood storage and mobility in large gravel-bed rivers, EPIC FORCE project Deliverable D20bis, http://www.tesaf.unipd.it/epicforce/Download.asp.

Dunford, R., K. Michel, M. Gagnage, H. Piégay, and M.-L. Trémélo (submitted), Potential and constraints of UAV technology for the characterisation of Mediterranean riparian forest.

Feldheim, K. A. (2002), Genetic tagging to determine passive integrated transponder tag loss in lemon sharks, *Journal of Fish Biology*, *61*, 1309-1313.

Gurnell A.M., Petts G.E., Harris N., Ward J.V., Tockner K., Edwards P.J., & Kollman J., (2000a). Large wood retention in river channels: The case of the Fiume Tagliamento, Italy. Earth Surface Processes and Landforms 25(3), 255–257.

Gurnell A.M., & Petts G.E., (2002). Island-dominated landscapes of large floodplain rivers, a European perspective. Freshwater Biology 47, 581–600.

Haga, H., T. Kumagai, K. Otsuki, and S. Ogawsa (2002), Transport and retention of coarse woody debris in mountain streams: An in situ field

experiment of log transport and a field survey of coarse woody debris distribution, *Water Resources Research*, 38, 1126.

Harris, S., W. J. Cresswell, P. G. Forde, W. J. Trewhella, T. Woollard, and S. Wray (1990), Home-Range Analysis Using Radio-Tracking Data - a Review of Problems and Techniques Particularly as Applied to the Study of Mammals, *Mammal Review*, 20, 97-123.

Haschenburger, J. K., and S. P. Rice (2004), Changes in woody debris and bed material texture in a gravel-bed channel, *Geomorphology*, 60, 241-267.

Hassan, M. A., D. L. Hogan, S. A. Bird, C. L. May, T. Gomi, and D. Campbell (2005), Spatial and temporal dynamics of wood in headwater streams of the Pacific Northwest, *Journal of the American Water Resources Association*, 41, 899-919.

Hughes, M. L., P. F. McDowell, and W. A. Marcus (2006), Accuracy assessment of georectified aerial photographs: Implications for measuring lateral channel movement in a GIS, *Geomorphology*, 74, 1-16.

Hyatt T.L., Naiman R.J. (2001), The residence time of large woody debris in the Queets River, Washington, USA., *Ecological Applications*, 11(1), 191-202.

Jackson C.R., & Sturm C.A., (2002). Woody Debris and Channel Morphology in First- and Second- Order Forested Channels in Washington's Coast Ranges. Water Resources Research 38:1177-1190.

Jacobson, P. J., K. M. Jacobson, P. L. Angermeier, and D. S. Cherry (1999), Transport, retention, and ecological significance of woody debris within a large ephemeral river, *Journal of the North American Benthological Society*, 18, 429-444.

Jones, T. A., and L. D. Daniels (2008), Dynamics of large woody debris in small streams disturbed by the 2001 Dogrib fire in the Alberta foothills, *Forest Ecology and Management*, 256, 1751-1759.

Keim, R. F., A. E. Skaugset, and D. S. Bateman (2000), Dynamics of coarse woody debris placed in three Oregon streams, *Forest Science*, 46, 13-22.

Keller, E. A., and T. Tally (1979), Effects of large organic debris on channel form and fluvial processes in the coastal redwood environment, in *Adjustments of the Fluvial System,* edited by D. D. Rhodes and G. P. Williams, 169-197, Kendall/Hunt, Iowa.

Kothyari U C, Ranga Raju K G 2001 Scour around spur dikes and bridge abutments. J. Hydraul. Res. 39: 367–374

Kraft, C. E., and D. R. Warren (2003), Development of spatial pattern in large woody debris and debris dams in streams, *Geomorphology*, 51, 127-139.

Lamarre, H., B. J. MacVicar, and A. G. Roy (2005), Using Passive Integrated Transponder (PIT) tags to investigate sediment transport in gravel-bed rivers, *Journal of Sedimentary Research*, 75, 720-725.

Landon, N., H. Piégay, and J. P. Bravard (1998), The Drome river incision (France): from assessment to management, *Landscape and Urban Planning*, 43, 119-131.

Lassettre, N. S., H. Piégay, S. Dufour, A.J. Rollet (2008), Decadal changes in distribution and frequency of wood in a free meandering river, the Ain River, France, *Earth Surface Processes and Landforms*, *33*, 1098-1112.

Lejot, J., C. Delacourt, H. Piégay, T. Fournier, M. L. Tremelo, and P. Allemand (2007), Very high spatial resolution imagery for channel bathymetry and topography from an unmanned mapping controlled platform, *Earth Surface Processes and Landforms*, 32, 1705-1725.

Lyn, D. A., T. Cooper, Y. K. Yi, R. Sinha, and A. R. Rao (2003), *Debris Accumulation at Bridge Crossings: Laboratory and Field Studies*. FHWA/IN/JTRP-2003/10, Indiana Department of Transportation and Federal Highway Administration, Purdue University, West Lafayette, Indiana.

MacVicar, B. J., H. Piégay, A. Henderson, F. Comiti, C. Oberlin, and E. Pecorari. 2009. Quantifying the temporal dynamics of wood in large river: field trials of wood surveying, dating, tracking, and monitoring techniques. *Earth Surface Processes and Landforms* 34: 2031-2046.

MacVicar, B. J., A. Hauet[2], N. Bergeron[3], L. Tougne[4] and I. Ali[4.] 2012. Chapter 16: River monitoring with ground-based videography. In P. Carbonneau et H. Piégay (Eds) : Fluvial remote sensing for science and management. J. Wiley and Sons.

MacVicar B., Piégay H., 2012. Implementation and validation of video monitoring for wood budgeting in a wandering piedmont river. Earth Surface Processes and Landforms.Wiley Online Library. DOI: 10.1002/esp.3240

Mao L, Burns S, Comiti F, Andreoli A, Urciolo A, Gavino-Novillo M, Iturraspe R, Lenzi MA. Acumulaciones de detritos lenosos en un cauce de Montaña de Tierra del Fuego: Analisis de la movilidad y de los efectos hydromorfologicos. In: Bosque, 29 (3); 2008. pp 197-211.

Moulin, B., and H. Piégay (2004), Characteristics and temporal variability of large woody debris trapped in a reservoir on the River Rhone (Rhone): Implications for river basin management, *River Research and Applications*, 20, 79-97.

Moulin, B., E. R. Schenk, and C. R. Hupp (2011), Distribution and characterization of in-channel large wood in relation to geomorphic patterns on a low-gradient river, *Earth Surface Processes and Landforms*, *36*(9), 1137-1151.

Pecorari, E. (2008), *Il materiale legnoso in corsi d'acqua a canali intrecciati: volumi, mobilità, degradazione ed influenza morfologica.* PhD Dissertation, Dept. Land and Agroforest Environments, University of Padova, Italy, 243 pp.

Piégay, H. (2003), Dynamics of wood in large rivers, in *Ecology and Management of Wood in World Rivers,* edited by S. V. Gregory, K. L. Boyer, and A. M. Gurnell, 109-134, American Fisheries Society, Bethesda, Maryland.

Sedell J.R., Bisson P.A., Swanson F.J., & Gregor S.V., (1988). What do we know about large trees that fall into streams and rivers?. in Maser, C., Tarrant, R.F., Trappe, J.M., and Franklin, J.F. (Eds.), From the Forest to the Sea: a Story of Fallen Trees. Pacific Northwest Research Station, USDA Forest Ser6ice, General Technical Report PNW-GTR-229, Portland. pp. 47–81

Seo, J. I., and F. Nakamura. 2009. Scale-dependent controls upon the fluvial export of large wood from river catchments. *Earth Surface Processes and Landforms* 34: 786-800.

Seo, J. I., F. Nakamura, and K. W. Chun. 2010. Dynamics of large wood at the watershed scale: A perspective on current research limits and future directions. *Landscape and Ecological Engineering* 6: 271-287.

Seo, J. I., F. Nakamura, D. Nakano, H. Ichiyanagi, and K. W. Chun. 2008. Factors controlling the fluvial export of large woody debris, and its contribution to organic carbon budgets at watershed scales. *Water Resources Research* 44: W04428.

Van der Nat, D., K. Tockner, P. J. Edwards, and J. V. Ward (2003), Large wood dynamics of complex Alpine river floodplains, *Journal of the North American Benthological Society*, 22, 35-50.

Wallerstein NP. 1998. Impact of LWD on fluvial processes and channel geomorphology in unstable sand bed rivers. Unpublished PhD thesis, University of Nottingham, UK.

Webb, A. A., and W. D. Erskine (2003), Distribution, recruitment, and geomorphic significance of large woody debris in an alluvial forest stream: Tonghi Creek, southeastern Australia, *Geomorphology*, 51, 109-126.

Wohl, E., and J. R. Goode (2008), Wood dynamics in headwater streams of the Colorado Rocky Mountains, Water Resources Research, 44, W09429.